Microscale Ionic Diodes: An Overview

Review

Wiley Online Library

ELECTROANALYSIS

DOI: 10.1002/elan.202060614

Microscale Ionic Diodes: An Overview

Budi Riza Putra,[a, b] Luthando Tshwenya,[c] Mark A. Buckingham,[d] Jingyuan Chen,[e] Koichi Jeremiah Aoki,[e] Klaus Mathwig,[f] Omotayo A. Arotiba,[c, g] Abigail K. Thompson,[a] Zhongkai Li,[a] and Frank Marken*[a]

Abstract: Ionic rectifier membranes or devices generate uni-directional ion transport to convert an alternating current (AC) ion current input into stored energy or direct current (DC) in the form of ion/salt gradients. Electrochemical experiments 80 years ago were conducted on biological membrane rectifier systems, but today a plethora of artificial ionic rectifier types has been developed and electroanalytical tools are employed to explore mechanisms and performance. This overview focuses on microscale ionic rectifiers with a comparison to nano- and macroscale ionic rectifiers. The potential is surveyed for applications in electrochemical analysis, desalination, energy harvesting, electrochemical synthesis, and in selective ion extraction.

Keywords: nanofluidics · voltammetry · electrolytic devices · iontronics · lab-on-a-chip.

1 Introduction to Microscale Ionic Rectifiers

Biomimetic single-pore or multi-channel ion transport processes are of considerable interest [1] and linked fundamentally to ionic rectifier behaviour. Fundamentally, a rectifier converts an alternating current (AC) input signal into a constant polarity direct current (DC) output signal. Rectifiers are based on diodes, which restrict current flow into only one direction [2]. Figure 1(A) demonstrates the effect of a single diode on the input signal essentially removing halve of the signal to leave a constant polarity output. Figure 1(B) illustrates the effect of a bridge rectifier (based on four coupled diodes) converting all of the AC input signal into a DC constant polarity output signal. Rectifier effects are very common in electrochemistry.

Electronic rectifiers are based on semiconductor or molecular electronic junctions with appropriate doping/structure to control flow of charge carriers at the interface [3]. Ionic rectifiers or diodes have been reported based on a range of different experimental approaches. There are macroscopic rectifiers based on electrolytic or nanopore array junctions [4] or chemical (switchable or analytical) junctions [5], micro-electrolytic interfaces [6] and microfluidic systems [7], and there are nano-electrolytic [8] as well as nanofluidic rectifier systems [9]. In contrast to electronic rectifiers that are based purely on transport of electrons, ionic rectifiers can be based on a wide range of mobile cation or anion species either with or without selectivity. Ionic rectifiers also link ion transport to electro-osmotic transport and are therefore suitable to uni-directionally "pump" neutral molecules [10,11]. It is interesting to explore the underlying fundamental similarities in diodes and **the two minimum conditions for diode behavior** to be observed:

Condition one: the experimental system has to be asymmetric. A symmetric system would not be able to generate an asymmetric output from a symmetric input signal. Asymmetric nanocones, asymmetric ionomer deposits, asymmetric external electrolyte solutions, asymmetric surface modifications, or other asymmetry inducing components are necessary (one type of asymmetry is sufficient). Asymmetry here refers to both absence of a mirror plane and absence of a center of inversion of the rectifier geometry. Note, that at the molecular scale this situation has important implications on enantio-selectivity of ion transport [12].

Condition two: a compositional and resistivity change has to occur as a function of applied voltage. Under

[a] B. Riza Putra, A. K. Thompson, Z. Li, F. Marken
Department of Chemistry, University of Bath, Claverton Down, Bath BA2 7AY, UK
E-mail: f.marken@bath.ac.uk
[b] B. Riza Putra
Department of Chemistry, Faculty of Mathematics and Natural Sciences,
Bogor Agricultural University, Bogor, West Java, Indonesia
[c] L. Tshwenya, O. A. Arotiba
Department of Chemical Sciences, University of Johannesburg,Johannesburg, Doornfontein, 2028, South Africa
[d] M. A. Buckingham
Department of Chemistry, Britannia House,
King's College London,
London, SE1 1DB,
UK
[e] J. Chen, K. Jeremiah Aoki
University of Fukui, Department of Applied Physics, 3-9-1 Bunkyo, Fukui,
9100017, Japan
[f] K. Mathwig
Stichting imec Nederland within OnePlanet Research Center, Bronland 10, 6708 WH
Wageningen, Netherlands
[g] O. A. Arotiba
Centre for Nanomaterials Science Research,
University of Johannesburg,
South Africa

steady state conditions, a diode can be represented (in a very simplified way) by a resistor that is variable as a function of the applied external voltage. For a resistor to change resistance, an internal compositional change is required (*e.g.* a change in charge carrier distribution, a change in electrolyte concentration distribution, a precipitation reaction, or change in orientation of molecular functional groups within ion channels, *etc.*).

To better illustrate the second condition, Figure 2 shows a schematic drawing of an ionic diode with the charge transport path hypothetically divided into microscopic resistor components (for solution, membranes, interfaces, *etc.*; assuming a system under steady state). Blue and grey regions are used purely to indicate asymmetry in materials without reference to any particular mechanism or scale. When changing the polarity of the applied voltage from positive to negative, at least one of these microscopic resistors (schematically representing interfaces, bulk materials, and regions in the device) needs to change to result in a net rectification effect. In a symmetric device, there would be no net change. In reality, all diodes (ionic or electronic [13]) exhibit properties that are associated with more complicated equivalent circuits (not just a sequence of resistors) that include

Budi Riza Putra received his B.S. degree (2010) and M.Sc. degree (2013) from Bogor Agricultural University Indonesia. He then obtained his PhD degree in electrochemistry in 2020 from the University of Bath UK.

Luthando Tshwenya is employed as a lecturer under the new generation academics program (nGAP) at the chemical sciences department of the University of Johannesburg. His research interests include the application of electromembrane processes and electrochemistry towards the development of new water, sensing and energy technologies.

Mark A. Buckingham achieved his MChem (Hons) Chemistry degree from the University of Bath in 2017 and is currently undertaking an electrochemistry Ph.D. at King's College London on the inherent limitations in thermogalvanic cells and inherently sustainable, earth-abundant redox couples.

Jingyuan Chem has completed her Ph.D from the University of Fukui (Japan) in 1996, supervised by Prof. Koichi Aoki. She has developed her expertise in "fundamental subjects of basic electrochemistry" with focus on the physics of interfacial phenomena.

Koichi Jeremiah Aoki currently works on fundamentals of electric double layer capacity relevant to dynamics and faradaic reactions, electric migration, and diffusion.

Klaus Mathwig received his Ph.D. in Physics from the Max Planck Institute of Microstructure Physics (Germany) in 2010. Currently, he is a Principal Member of Technical Staff at the OnePlanet Research Center / imec Netherlands. His research focuses on microfluidic electrochemical sensing.

Omotayo A. Arotiba is a Professor of Chemistry at the Department of Chemical Sciences and the Director of the Centre for Nanomaterials Science Research at the University of Johannesburg, South Africa. His research interests are in the application of electrochemistry/photo-electrochemistry in sensors, biosensors, water treatment, materials science and nanotechnology.

Abigail K. Thompson is in her final year of a Ph.D. in sustainable applications of electrochemistry, at the Centre for Sustainable and Circular Technologies (CSCT), University of Bath.

Zhongkai Li obtained a B.Eng. in Chemical Engineering and Technology at Tongji University (China), an M.Sc. in Analytical and Pharmaceutical Science at Loughborough University (UK), and is now a Ph.D. researcher at the University of Bath (UK).

Frank Marken (Dr. rer. nat. RWTH Aachen, Germany) worked as a Stipendiary Lecturer at the University of Oxford (UK) before moving to the University of Loughborough (UK), and then being appointed at the University of Bath (UK).

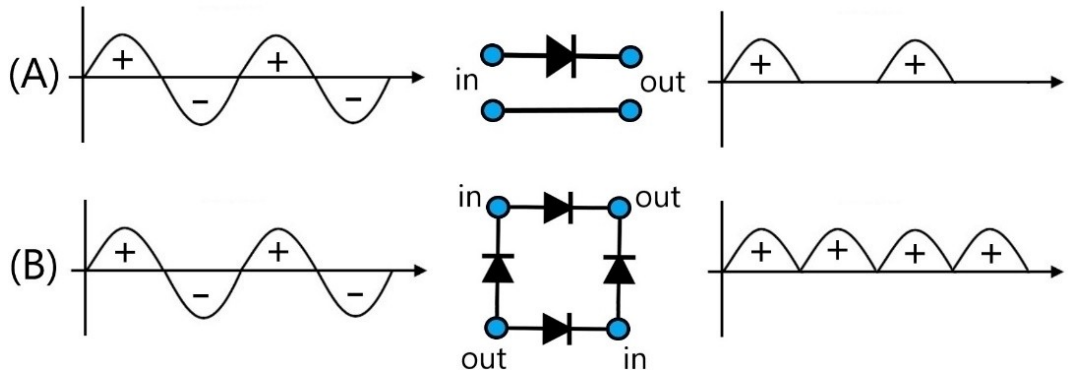

Fig. 1. (A) Effect of a diode on a sinusoidal input signal. (B) Effect of a rectifier on a sinusoidal input signal.

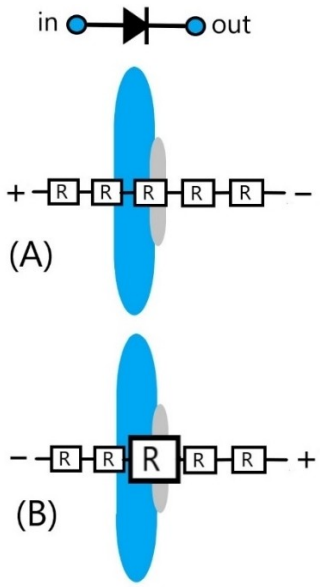

Fig. 2. Schematic description of the steady state behaviour of a diode as sequence of resistors with at least one resistor showing voltage/polarity dependent resistance caused by compositional changes. A blue and a grey material are indicated here generally to illustrate asymmetry with the grey material only on one side of the device.

capacitive interfaces and components, which are important when describing the transient or frequency-dependent switching behaviour. At higher frequencies diodes lose their ability to switch and to rectify current signals. This can be interpreted as the compositional change requiring time. The **time constant** for the diode to switch from inactive to active is an important operational characteristic [14] (*vide infra*).

Early studies of rectification effects in electrochemistry [15,16] and in electrophysiology were mainly concerned with biological processes [17,18]. Membranes in neuron cells have uni-directional ion channels [19]. These membranes were mounted between two electrolyte-filled compartments, and the membrane rectification properties were measured using a sinusoidal voltage source. Rectification was shown to decrease reversibly under the influence of increased salt concentrations. In the 1950s, Hodgkin, Huxley and Keynes studied sodium and potassium passage through giant axons against a concentration gradient. Their hypothesis was: when the nerve fibres of these species are stimulated, they undergo rapid changes in permeability, which can allow sodium and potassium ions to move down concentration gradients, while co-ions are effectively blocked [20,21,22]. This leads to propagating neve signals. Biological ion-channels provide a wide range of mechanistic cases with complex systems resulting in the movement of nerve pulses and energy conversion [23].

Biological diodes and pioneering experiments. An example of biological pore diodes is the family of inward-rectifying potassium channels [24] or more specifically OmpF (outer membrane protein F), which have been studied for ionic rectification effects [25]. The inner protein channel (which is part of an external membrane protein channel in *Escherichia Coli* bacteria) has surface charges and may therefore be considered as an "electrostatic" diode, which can be tuned or even inverted using pH (see Figure 3). Surface charges determine the ability of cations and anions to enter the ion channel and this leads to either depletion (high resistance) or accumulation (low resistance) conditions.

Inspired by rectification in electronic junctions between p- and n- type semiconductors, electrolytic systems combined with artificial membranes were investigated in the 1950s. Work by Fuller [26], and particularly by Lovrecek *et al.* [27] showed that a combination of proton-conducting and hydroxide-conducting semi-permeable membranes separating two reservoirs filled with identical electrolyte solution (*i.e.* water) results in ion current rectification (see Figure 4). Similar to a p-n-junction this bipolar membrane (*i.e.* the combination of a cation- and anion- exchange membrane) creates conditions of "depletion" and of "accumulation" of charge carriers (as voltage dependent compositional changes).

Figure 4(A) illustrates the mechanism [27]. With forward bias, both cations and anions are driven into the cation exchange membrane and anion-exchange mem-

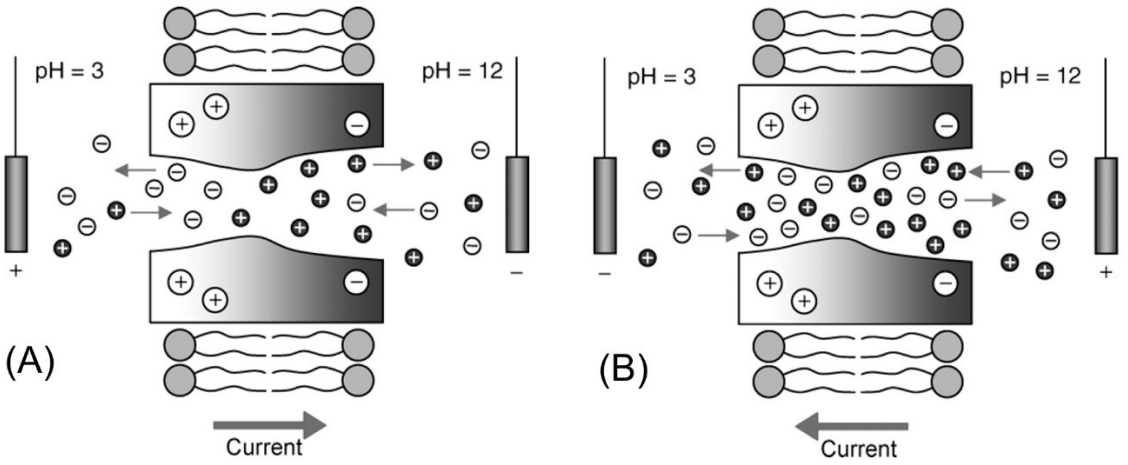

Fig. 3. Schematic representation of the bipolar diode effect in a natural ion channel (OmpF protein) under positive applied potential (A) and negative bias (B) and in the presence of a pH gradient. Reprinted with permission from [25]. Copyright (2006) American Chemical Society.

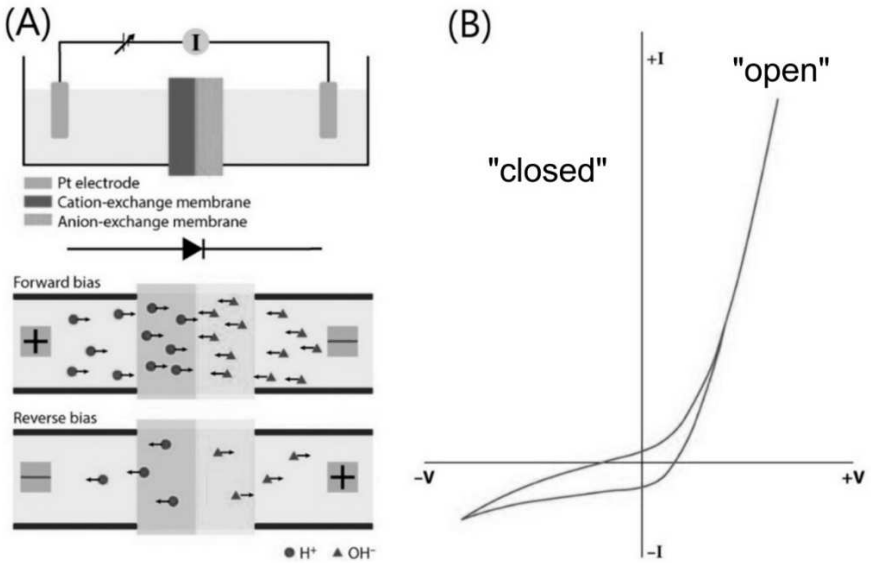

Fig. 4. (A) Illustration of how rectification effects can be formed by transport of cations/anions through semi-permeable cation-/anion-selective films. Reprinted with permission from [111]. Copyright (2015) Annual Reviews. (B) A typical *I–V* current curve with rectification effect seen experimentally. Reprinted with permission from [27]. Copyright (1959) American Chemical Society.

brane, respectively, which forms the semipermeable membrane. Ions accumulate in this junction region. Thus, in all parts of the system the resistance remains low. Note that this accumulation in forward bias lowers the local Debye length to allow not only salt accumulation but also continuous flow of ion current. In contrast in reverse bias, cations and anions are removed from the junction region and depletion of ions results in a zone of high resistance in the ion-exchange membrane. Both conditions are met: there is (one) asymmetry and (two) a compositional change that occurs to generate the typical diode response. Figure 4(B) shows a current-voltage response with "open" state with positive applied potential and "closed" state with negative applied potential.

Over the years, the concept of rectification in electrochemistry has been studied and exploited [29]. The concept of ionic rectifiers and diodes has been developed into ionic circuits [30], ionic transistors [31], ionic amplifiers [32], and a range of potential ionic diode applications. In the following sections, the various types of ionic rectifiers or diodes are compared, and some possible future applications in electrochemistry and in electroanalysis are discussed.

2 Nanopore Electrolytic and Nanofluidic Ionic Rectifiers

It is possible to distinguish electrolytic diode devices (based on ionomer junctions) and fluidic devices (essentially open channels with electroosmotic flow). However, at the limit of nanopore devices, this distinction becomes obsolete with device sizes similar to the Debye length in the solution phase. Many studies focus on bio-derived nanopores with molecularly defined geometry [33]. In contrast, artificial solid state nanopores can be machined into wafer materials [34] or developed based on "track etch" membranes [35]. In such membranes, solid-state nanopores provide well-defined nanochannels made from thin synthetic films or membranes by heavy ion track formation followed by etching [36]. Compared with biological nanopores, solid-state nanopores are mechanically robust and durable with a tuneable pore size and geometry (but without the molecularly reproducible geometry as seen in biological systems).

Synthetic membranes with artificial and well-defined nanopores (solid-state nanopores) that behave similarly to biological membranes, were first reported by Siwy and coworkers in 2002 [37]. These solid-state nanopores are fabricated on track etched polymers (see Figure 5). During this track-etch process, an asymmetric pore is readily formed, which can be subsequently altered to different shapes of different diameters and surface charge using chemical means [38,39,40,41]. The ester functional groups normally present in polyester substrates such as polyethylene terephthalate (PET) can easily be converted to carboxylates, which under alkaline pH conditions

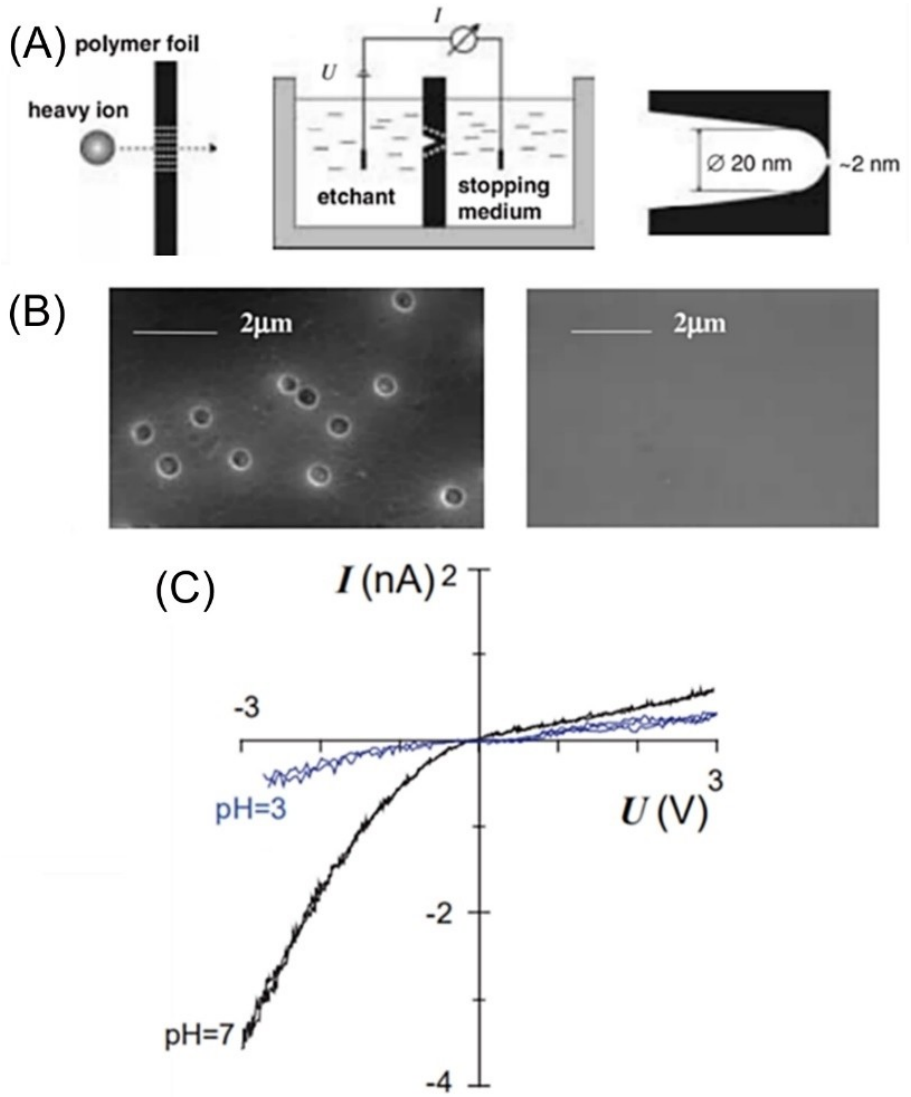

Fig. 5. (A) The principle of fabricating conical nanopores using the track-etching technique. (B) SEM images of two surfaces (top and bottom) of a PET membrane with fabricated conical pores. The narrow opening of the conical pores is below SEM resolution, and thus cannot be seen. (C) *I–V* curves for the conical nanopore at 0.1 M KCl and different pH conditions, rectification is only observed at pH 7 due to surface charges. Reprinted with permission from [37]. Copyright (2002) EDP Sciences.

produce negative surface charges that can assist in the conduction of positively charged species while blocking voltage driven anion transport. The asymmetry in shape of the nanopore, together with the carboxylate surface charges after chemical etching, has been found (by experiment and by theory) responsible for the diode-like behaviour of these nanopores [42]. Microfabricated arrays of longer (>100 μm) nanochannels with an asymmetry of fixed surface charges deposited along the channel walls have been demonstrated to form efficient nanofluidic diodes [43].

Recent studies include for example nanofluidic diodes [44] in which CO_2 and N_2 are used to "open" and "close" the diode state of a conically shaped nanopore in a PET membrane. CO_2 is used to protonate the imidazole group (see Figure 6). The pH is regulated by a buffer mechanism based on CO_2 dissolution. Purging with nitrogen can be used to reverse the pH and the diode state. This work is related to olfactory sensory neurons that are specialized for sensing CO_2 [45,46] biologically. The switch of the diode is reversible if N_2 is bubbled through the nanopore.

A new strategy for generating ionic current rectification through larger microscale pores was introduced in 2010 by Yusko *et al.* [47]. Ion current rectification was coupled to electroosmotically driven flow of liquids of varying viscosity into/out of pores with diameters ranging from 0.01 μm to 2.2 μm on borosilicate glass of 150 μm thickness. This method does not require spatially patterned surface charges, ionic gradients, or pores with a dimension on the order of the Debye screening length to generate ion current rectification. Instead, the asymmetry necessary for rectification is achieved by relying on different ion conductivities in liquids of different viscosities at both ends of a cylindrical micropore [45].

Extending the concept of fluidic diodes to the micropore range could be of interest for applications, such as desalination and energy conversion. Today, a variety of ionic diode concepts based on micro-interfaces are available and have been shown to work in larger microhole devices with diameters up to 40 μm, with sometimes better rectification performance than observed for devices based on nanopores [48]. Nanofluidic crystals and close-packed nanoparticle arrays have been developed [49]. Diode phenomena in confined nano-spaces have been exploited for bioanalysis and label-free sensing [50].

An ionic diode that rectifies or allows passage of cations while blocking anions may be called a "cationic diode". A diode that rectifies anion flow instead of cation flow may be called an "anionic diode". These two types of cases are observed in different types of devices. Figure 7 shows typical *I–V* curves for microfluidic ion channel measurements in organic solvent systems in the presence of electroosmotic flow [51]. For a channel of 700 nm diameter, it was shown that the surface charge could be switched from negative (native PET) to positive (with adsorbed poly-allylamine). Due to the dimensions of the

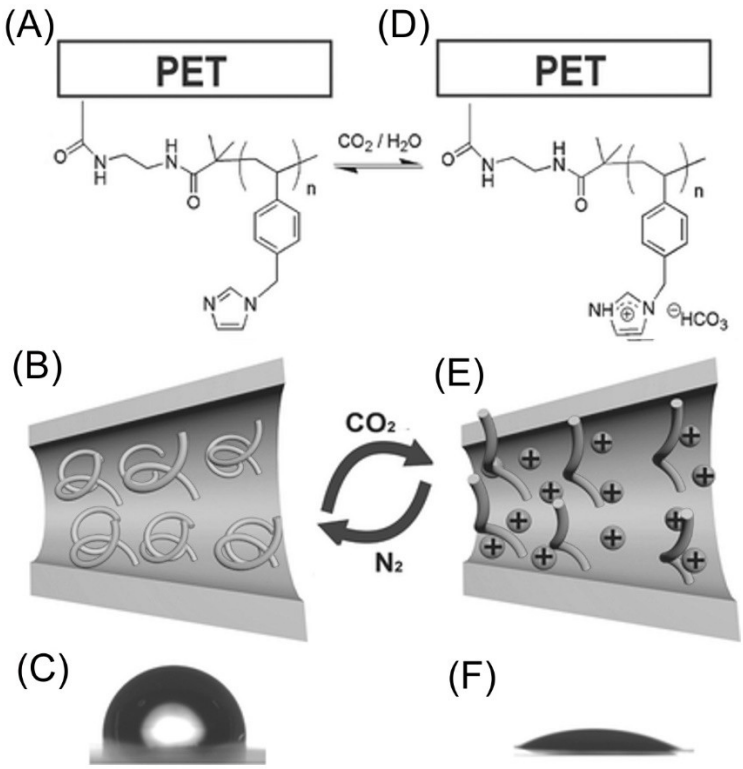

Fig. 6. The protonation of the PET-surface-attached imidiazole group upon introduction of CO_2 causes ionic diode switching and surface wetting changes. (A–C) Before exposure to CO_2. (D–F) The effect is reversed by purging with dinitrogen. Reprinted with permission from [44]. Copyright (2015) Wiley.

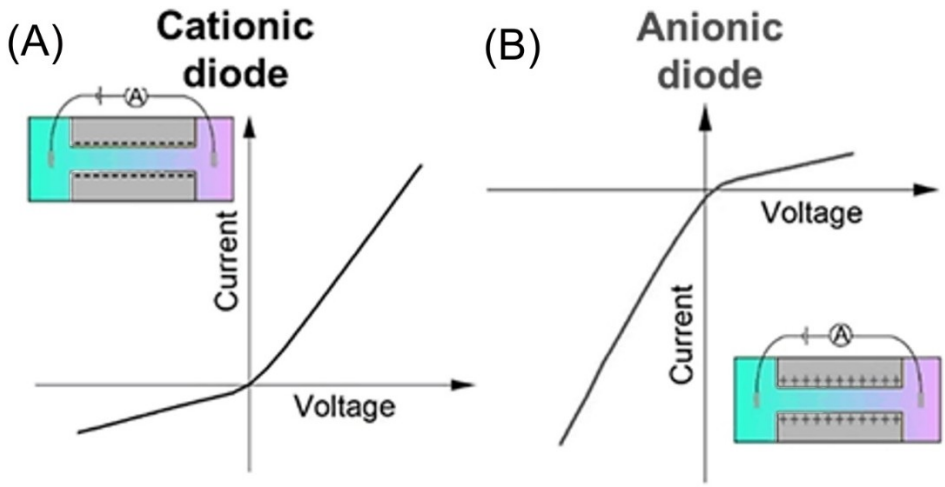

Fig. 7. (A) *I–V* characteristics for a negatively charged channel and (B) for a positively charged channel to contrast cationic diode and anionic diode behaviour in cylindrical channel. Reprinted with permission from [51]. Copyright (2019) American Chemical Society.

ion channel, it is apparent that ion currents in this case will contain contributions from both anion transport and cation transport, as well as contributions from electro-osmosis (flow of neutral electrolyte solution). However, the net process appears to be dominated either by cations (cationic diode) or by anions (anionic diode). The region with high current can be called the "open" state of the diode, while the region with suppressed currents can be called the "closed" state. To evaluate the rectification ratio of the device (the diode performance), a ratio of ionic currents is taken at opposing voltages of the same magnitude (+/−1 V), and the higher the ratio is, the better the diode performance or rectification ability.

The distinction between "cationic diode" and "anionic diode" is very useful as a diagnostic tool and often the switch from one type to the other type has been shown to occur when the surface charge is changed (*e.g.* when changing the pH of the electrolyte solution). However, it is important to remember that the transport of protons and the transport of hydroxide are chemically equivalent. Therefore, a cationic proton diode and an anionic hydroxide diode cannot be easily distinguished simply from steady state *I–V* curves and identifying the mechanism in this case would require further, more detailed experiments. Therefore, the *I–V* curve is not necessarily reliable as a diagnostic mechanistic tool.

In electroanalysis, biological nanopore sensors have been exploited for detection of nucleic acids and for DNA quantification. For artificial solid state nanopores, it has been shown that surface modification and charge are important for electroanalytical detection. For example, with a positively charged ion channel, increasing the DNA concentration in solution may cause adsorption, which is associated with a dramatic shift in the *I–V* curve from a dominating positive current to a dominating negative [52] (see Figure 8). When working with a glass nanopipette, an overall negative wall charge repels the DNA strands. A poly-L-lysin (PLL) layer needs to first be adsorbed onto the nanopipette to produce a net positive charge, with which the DNA can be attracted and detected. The change in surface charge due to DNA binding leads to switching of the diode effect (see Figure 8). The effect has been demonstrated with multiple consecutive layers of PLL and DNA.

In contrast to the case of electronic diodes, specificity between ions is important for the case of ionic diodes. There have been attempts to employ molecular dynamics simulations to mimic the selectivity in biological pores, namely K^+/Na^+ channels in artificial graphene-type structures. Thus, this work is addressing one of the most important challenges in ion separation. These *in silico* functionalised nanopores are proposed to be made from graphene sheets that contain pores. These pores then have the potential to be "ionic sieves" with selectivity and, by chemical modification the capability of being either cation or anion selective [53]. The calculated selectivity depended on the terminating group arrangements, for example the carboxyl arrangement being selective between Na^+ and K^+ ions. The introduction of 4 carboxylate and 4 carbonyl groups increased the selectivity towards K^+ [54]. The functionalised pore with 3 carboxylate groups has been proposed to exhibit Na^+ selectivity [55,56] (see Figure 9). The corresponding asymmetric ion channels would provide ionic diode phenomena.

3 Macro-electrolytic and Chemical Ionic Rectifiers

Classic work by Lovrecek and Bockris has shown that hydrogel | hydrogel interfaces create macrosocpic rectifying junctions [27]. This effect has been confirmed for different types of ionomer junctions [57] and it is not limited to small or nano-scale devices. Both hydrogel junctions and arrays of nanocones can be employed to prepare ionic diode devices for higher currents. Nevertheless, hydrogels have been employed also for ionic

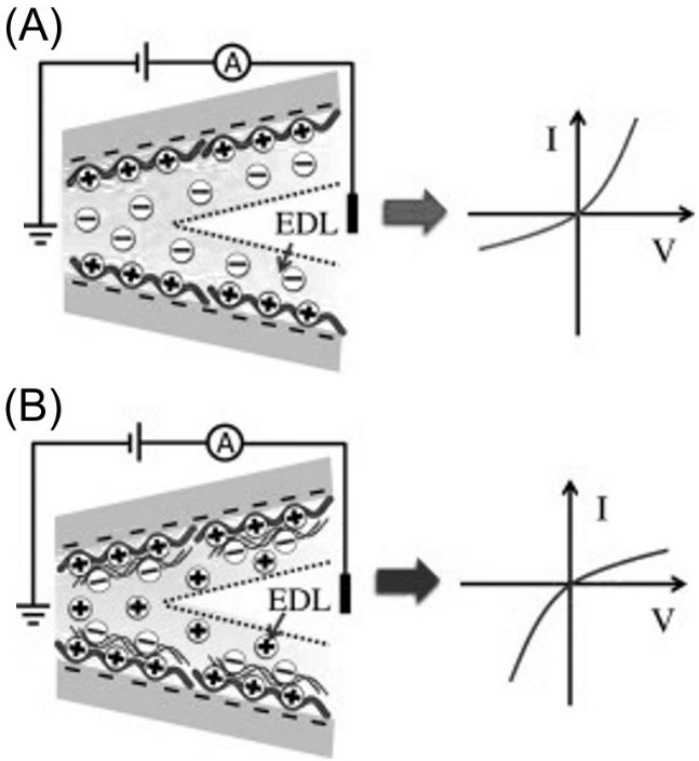

Fig. 8. Schematic description of a switch from anionic diode to cationic diode due to DNA adsorption. A cross section of the conical nanofluidic diode profile. (A) With a positive surface charge (adsorbed polyelectrolyte poly-L-lysine PLL) anion transport dominates. (B) When the DNA is adsorbed onto the PLL layer cation transport dominates. Reprinted with permission from [52]. Copyright (2013) Elsevier.

rectification in combination with conical nanopores [58]. The hydrogel has the effect of increasing the diode effect only for "tip coatings" but decreasing the rectification effect for "base coating" and coating on both sides (see Figure 10). With this particular nanopore having an overall negative charge, it was showing rectification effects of cation selectivity without the hydrogel. One intriguing aspect of this research is that improved rectification was only achieved when the hydrogel was introduced at the tip of the cone, and not for the other arrangements (illustrated in Figure 10).

"Chemical diodes" are ionic diodes that rely on chemical processes, instead of relying on purely physical phenomena. These chemical processes, such as precipitation are utilized to induce ionic rectification effects. Chemical diodes can be very novel in the way that they have been found in non-water-based liquid electrolytes [59]. Usually, for ionic diode behavior to be observed the electrolyte medium is water-based, where the ionic solutes can dissociate easily and conduct upon flow of a current. In this example (Figure 11) poly-ethylene-oxide (PEO 400) was used as the electrolyte medium and AgI was the precipitate created at the interface of two compartments. The AgI precipitation caused a "chemical blocking" of the ionic current in the diode.

4 Microscale Ionic Rectifiers: A Materials Approach

Rectification phenomena have been investigated predominantly with a focus on nanoscale channels. Based on this, it may seem that effects are difficult to achieve when the pore diameter is more than 10 times larger than the Debye screening length. However, rectification effects are also commonly observed for microhole devices [60] and for larger electrolytic junction diodes. Yossifon and coworkers developed microfluidic diodes [61] as well as poly-electrolyte-based microfluidic ionic rectifiers [62]. In larger open channels (*e.g.* in micropipettes) the flow of ions is accompanied by electroosmotic flow and both ion current and electroosmotic transport can be rectified [10,63,64,65]. A hybrid system can be introduced (to suppress electroosmotic flow) by combining a microhole with ionomer materials.

A relatively simple experimental approach for developing microscale ionic diodes can be based on inert microhole substrates that are coated *asymmetrically* with ionomer materials. Semi-permeable ionomer materials, when deposited onto an inert poly-ethylene-terephthalate (PET) substrate with a laser-drilled microhole, were shown to give ionic diode effects [66]. The use of laser-drilled PET substrates for studying liquid | liquid phase boundary processes was introduced by Girault and co-

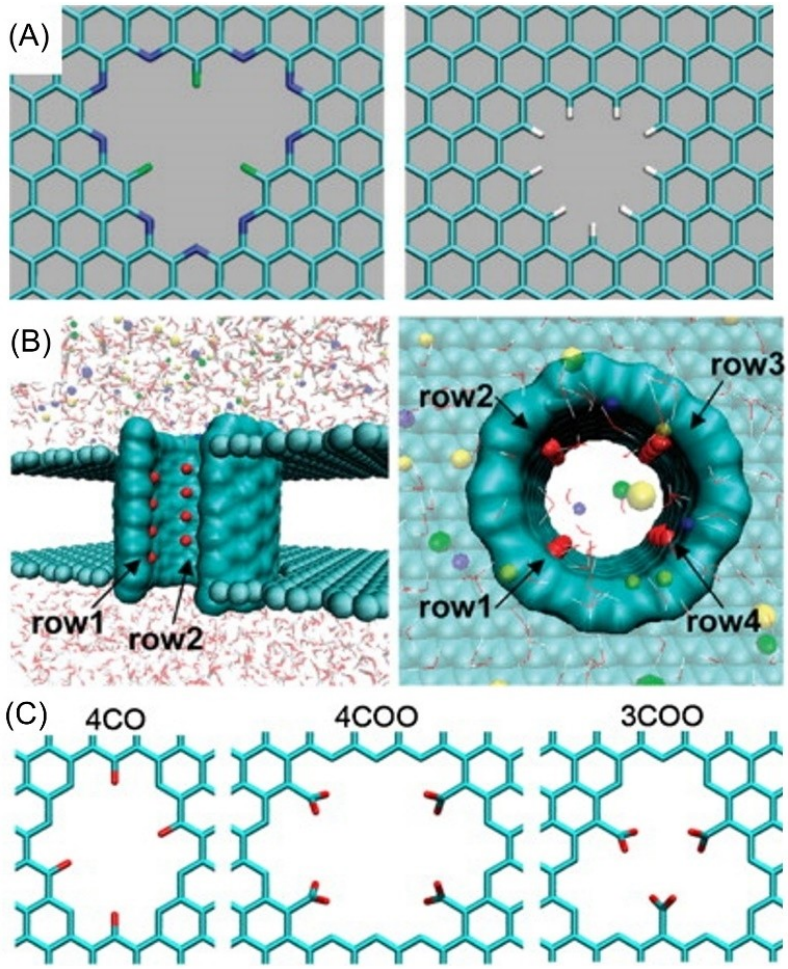

Fig. 9. (A) Representation of N and F terminated (left), or H terminated (right) ion channels; (B) carbon nanochannel modified by carbonyl groups in a membrane studied by MD simulations; (C) graphene nanopores etched and terminated for selectivity towards K^+/Na^+. Reprinted with permission from [55]. Copyright (2015) Elsevier.

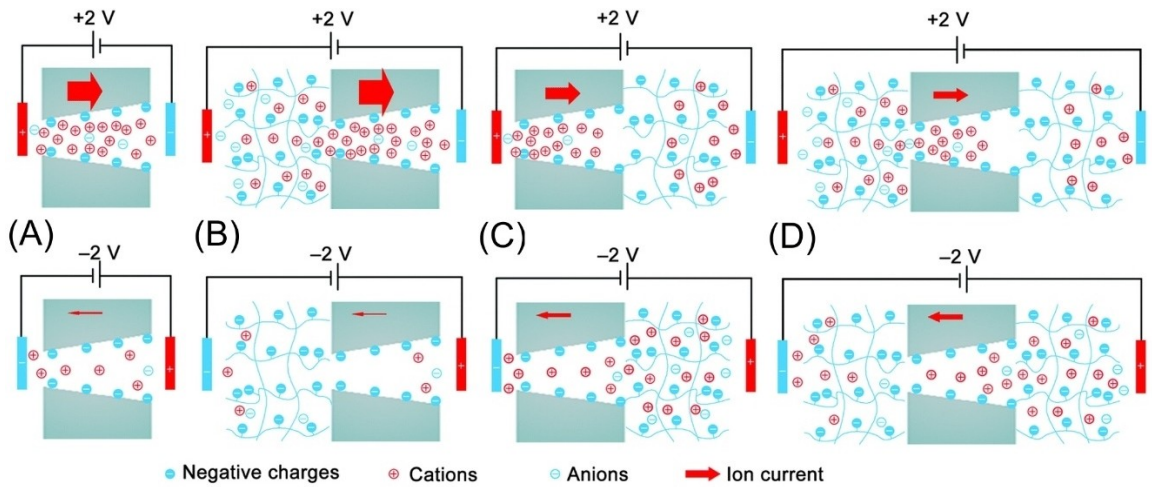

Fig. 10. Schematic for the rectification effects (A) without hydrogel, (B, C) with hydrogel on one side, and (D) with hydrogel applied on both sides of a nanocone. The −2 V case corresponds to the 'closed' diode current and the +2 V case corresponds to the 'open' diode current. Only hydrogel applied to the small orifice of the cone can significantly enhance the rectification effect. Reprinted with permission from [58]. Copyright (2015) Royal Society of Chemistry.

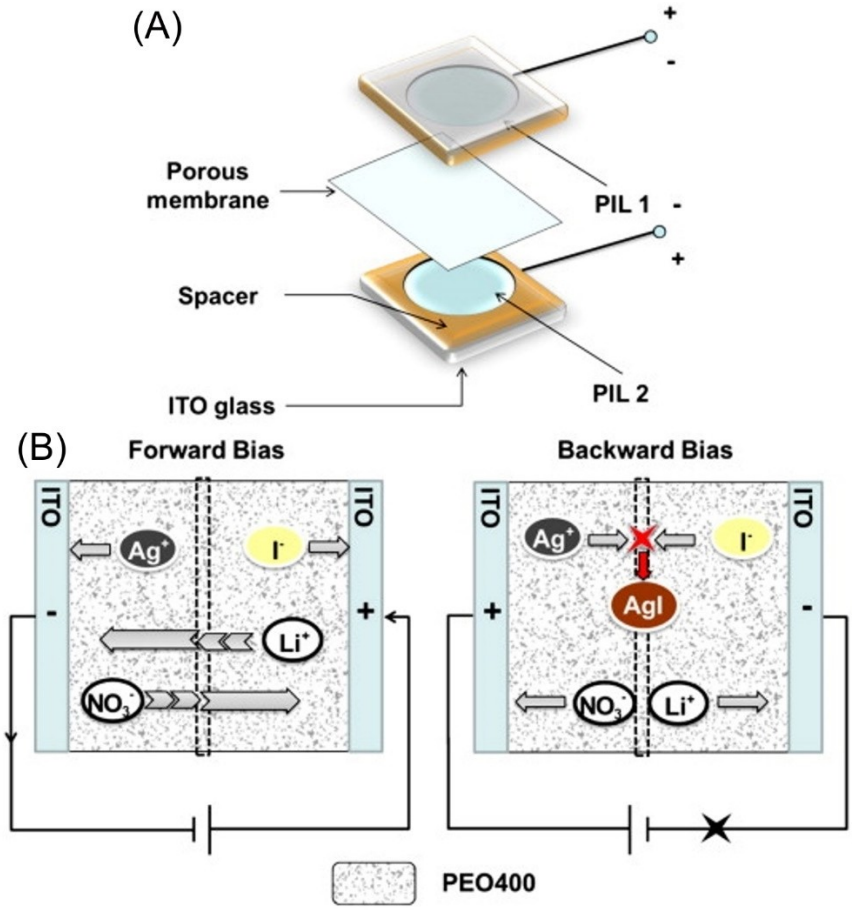

Fig. 11. (A) Illustration of the two-compartment device with porous membrane separator. (B) Mechanism for creating a "chemical" diode effect due to depositing salts on the central membrane. Reprinted with permission from [59]. Copyright (2012) Elsevier.

workers [67] as a tool to create stable interfaces, to restrict current flow, and to ensure steady state conditions similar to those observed at microelectrodes [68]. Note, that all liquid | liquid phase boundaries are inherently asymmetric and could be considered as ionic current rectifier systems [69]. However, here the practically relevant case of aqueous solution phase on both sides of the microhole is considered. Figure 12(A) shows an optical micrograph for a single 20 µm diameter laser-drilled microhole and for an array of 100 microholes (employed to increase the net current through the rectifier). Figure 12(B) shows the classic four-electrode

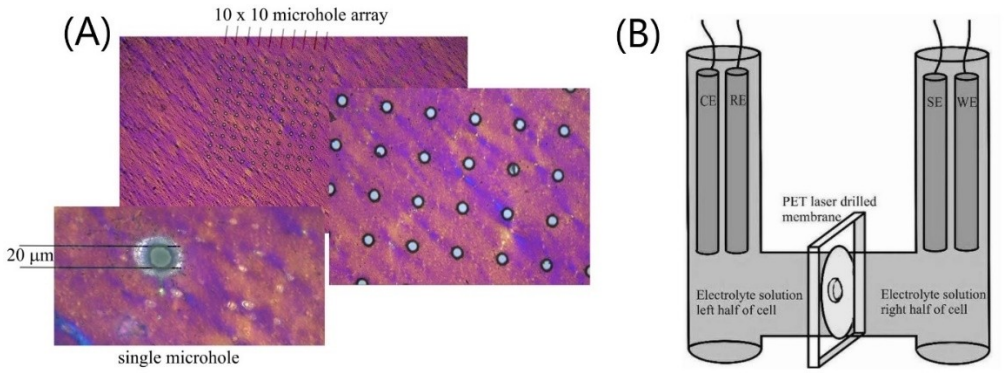

Fig. 12. (A) Optical micrograph showing a 20 µm thick PET substrate with a single microhole or a 10×10 microhole array laser drilled with approx. 20 µm diameter. To produce ionic diode effects, one side of the PET film is coated with ionomer. (B) Experimental four-electrode electrochemical membrane cell. Reprinted with permission from [66]. Copyright (2020) Elsevier.

experimental configuration for membrane electrochemistry employing two reference electrodes (RE reference electrode; SE sense electrode) to set the applied voltage bias and two current carrying electrodes (CE counter electrode; WE working electrode).

A single microhole (or several) is drilled in PET films using a laser device, then an ion-conducting microporous material is deposited onto one side of the microhole to introduce asymmetry and semi-permeability. Practically, this can be achieved by placing the PET film onto an agarose gel that blocks the back and that allows asymmetric ionomer casting onto the front side only. The microhole, in the absence of any deposited microporous material results in linear Ohmic current-voltage plots consistent with the bulk resistivity of the aqueous electrolyte [70]. When coating both sides equally, for example with the ionomer Nafion [71] (see Figure 13(A)), again ohmic current-voltage behaviour (without rectification) is observed, although with a lower resistance due to a higher concentration of charge carriers in the microhole region. Only when coated asymmetrically (see the red line in Figure 13(B)) is an ionic diode effect observed. Nafion has fixed sulphonate functional groups in 1 to 4 nm diameter channels and therefore allows semipermeable cation transport. Data in Figure 13(C) demonstrate the cases of a Na^+ diode and a H^+ diode.

Electrochemical impedance spectroscopy offers a powerful tool to explore the non-steady state aspects of the ionic diode behavior. Figure 13(D) shows a Nyquist semi-circle consistent with the interfacial charging of the PET film and the high frequency resistance of the diode. Only when going to lower frequencies and for asymmetric devices (Figure 13(F)) can a second semi-circle be observed linked to the time constant for diode opening/closing.

In order to gain further insight into the diode mechanism, approximate computational models can be employed. Figure 14 shows and illustrates the case of Nafion deposited asymmetrically onto a 20 µm diameter microhole and immersed into aqueous NaCl [72]. Figure 14(C) shows the calculated cation concentration (red) and anion concentration (blue) across the diode and comparing the "open" and the "closed" states. The open state is associated with electrolyte accumulation into the microhole region and the closed state is associated with electrolyte depletion from the microhole region. Both effects occur due to the system trying to maintain electroneutrality during ion current flow. Therefore, both

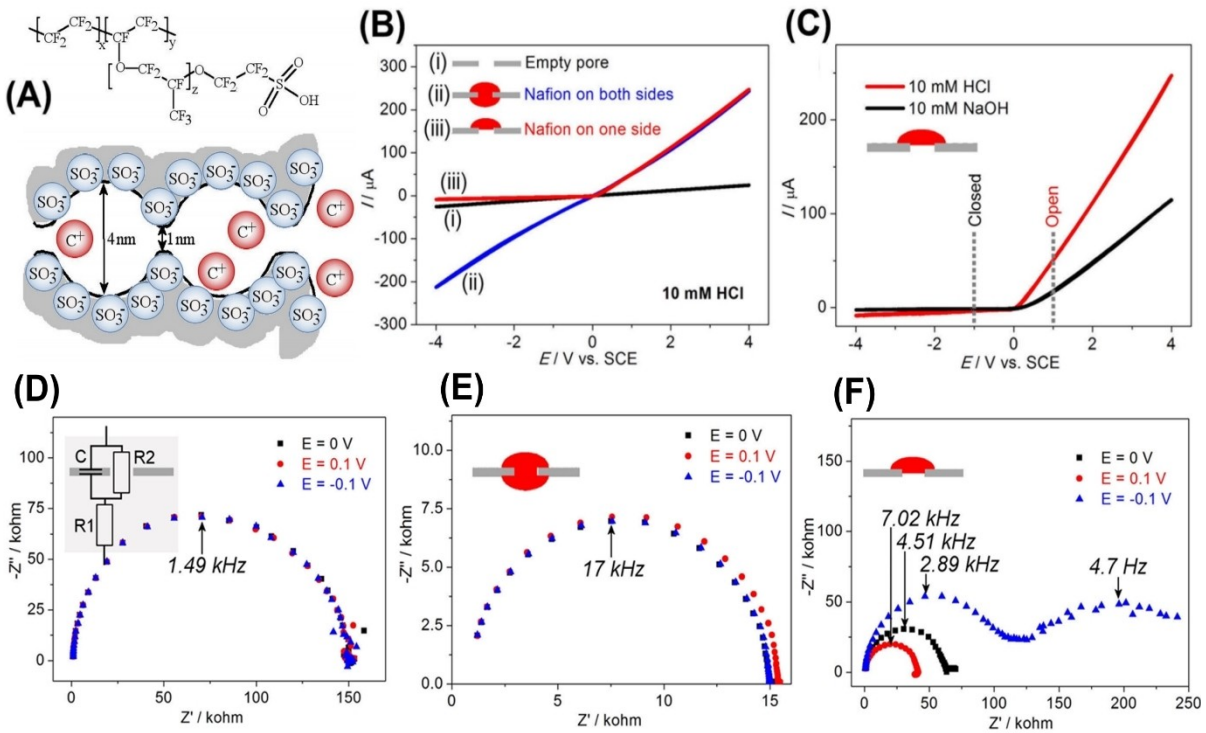

Fig. 13. (A) Molecular structure of Nafion with ion channels for cation conduction. (B) Current-voltage curves (scan rate 0.05 $V s^{-1}$) in aqueous 10 mM HCl comparing an empty microhole, a symmetrically coated microhole, and an asymmetrically coated microhole. (C) Cationic diode effects for aqueous 10 mM HCl and 10 mM NaOH. (D–F) Electrochemical impedance data (frequency range 100 kHz to 1 Hz; amplitude) for a 20 µm diameter microhole in PET immersed into 10 mM HCl on both sides compared to data obtained with symmetric and with asymmetric Nafion deposits. Data are shown for (D) the PET microhole without Nafion, (E) the microhole with Nafion applied to both sides, (F) the microhole with Nafion applied asymmetrically to only one side (reproduced with permission [71]). Reprinted with permission from [71]. Copyright (2017) American Chemical Society.

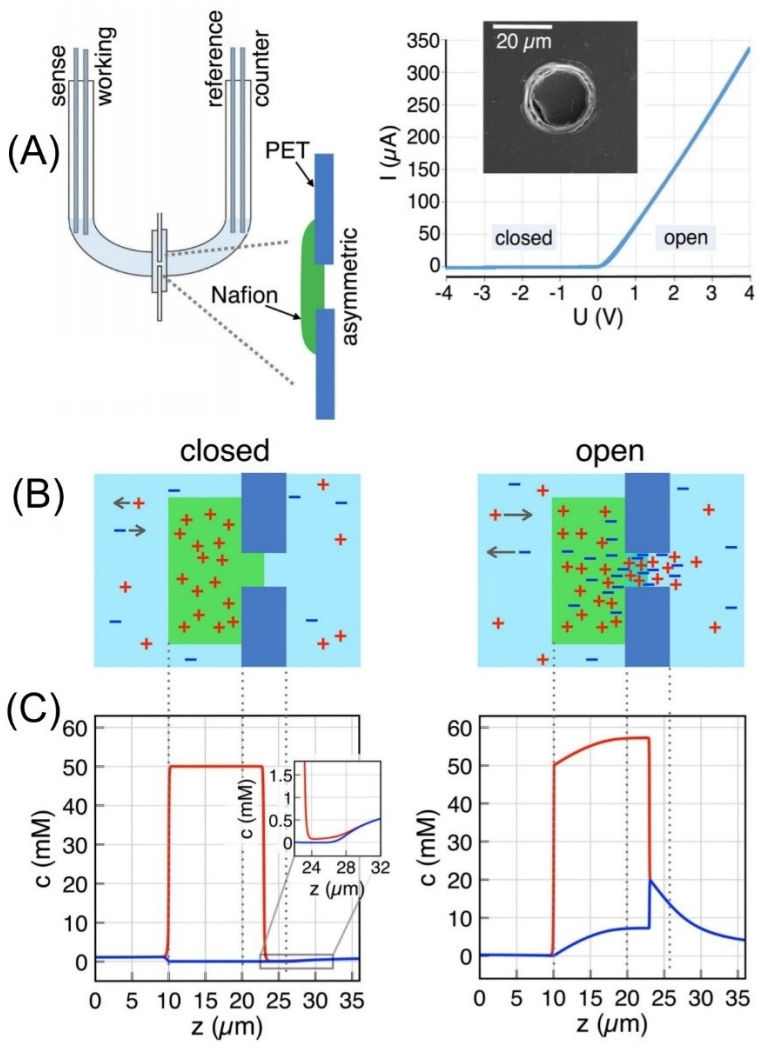

Fig. 14. (A) Illustration of the experimental cell with Nafion ionomer deposited onto a 20 μm diameter microhole on the side of the working electrode and a typical current voltage cure obtained in aqueous 10 mM HCl with a scan rate of 10 $mV s^{-1}$. (B) Schematic drawing of cation/anion populations during closed/open diode states. The green surface indicates the Nafion membrane with fixed negative charges. (C) Computational data for the case of closed and open diodes. Reprinted with permission from [72]. Copyright (2018) Wiley.

asymmetry and a compositional change are necessary to create the ionic current rectification effect.

In other words, in the closed state anions are quickly driven out of the microhole region by migration within the electric field; this now ion-deficient microhole region cannot be resupplied from the ionomer membrane as it is depleted of mobile anions. At the same time, cations leave the microhole constriction by comparatively fast migration into the negatively charged Nafion ionomer membrane, driven by migration as well as a strict condition of electroneutrality. From the ionomer, they also exit easily into the reservoir due to the large boundary surface area – thus avoiding out-of-equilibrium accumulation in the membrane. Consequently, the microhole volume is depleted of both cations and anions, where any current across it is subsequently blocked. In contrast, in the open state anions are driven by the electric field from the reservoir into the microhole, where they accumulate as the passage further into the negatively charged ionomer is hindered. Simultaneously, the ionomer acts as an efficient source of cations which also accumulate in the microhole, enabling the high open-state ionic current.

While the size of the microhole by far exceeds any Debye layer, the ionomer-microhole compound nonetheless acts as a fluidic diode, as the accumulation/depletion of ions in this bottleneck-area – determined by the asymmetrically positioned microporous membrane – overall yields a high or low conductivity.

A more general but simplified analytical model for ionomer coated microholes was developed by Aoki and Chen based on experimental data obtained with an ionic diode based on graphene oxide [73]. Figure 15(A) shows the experimental arrangement with graphene oxide asym-

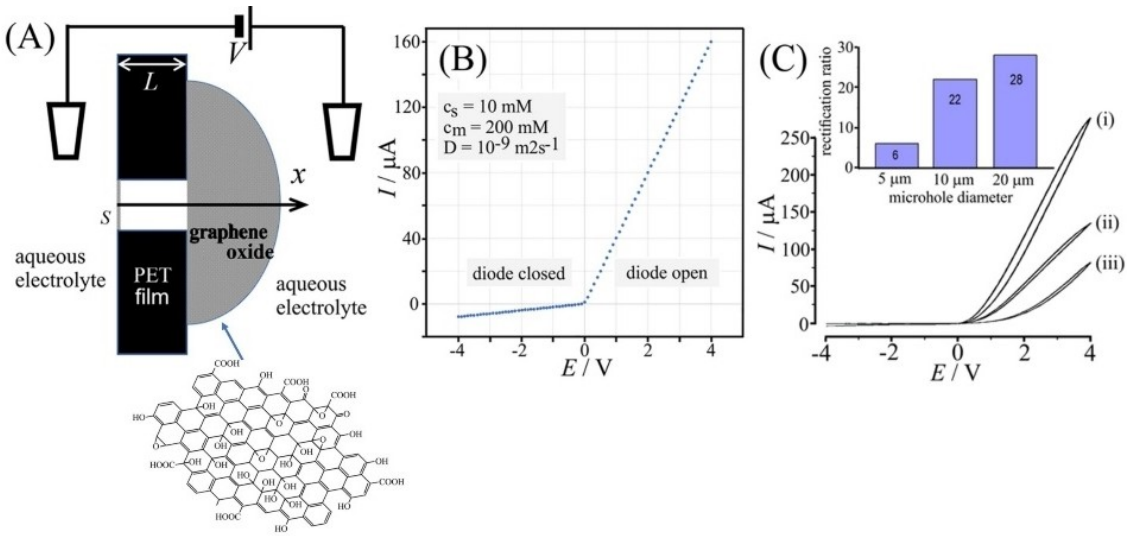

Fig. 15. (A) illustration of the cylindrical microhole region between bulk electrolyte (surface S) and ionomer deposit (in direction x). (B) Calculated current-voltage dependency based on equation 2. (C) Experimental I–V data for a graphene oxide coated microhole with scan rate 50 mV s^{-1}, immersed in 10 mM HCl. Reprinted with permission from [73]. Copyright (2019) American Chemical Society.

metrically deposited onto the PET substrate. Figure 15(B) shows a plot of equation 1 for the ionic diode current, I, derived by assuming fixed concentration c_s and c_m (for external bulk solution and for the membrane, respectively) and that electroneutrality must be maintained within the microhole region.

$$I = (AF^2D\phi_L/LRT)(c_m\text{-}c_s e^{-u})/(1\text{-}e^{-u}) \quad (1)$$

In this expression $u = F\phi_L/RT$ with ϕ_L being the externally applied voltage. A is the area of the cylindrical micropore, F is the Faraday constant, D is the diffusion coefficient for the electrolyte cation/anion, L is the length of the microhole, R is the gas constant, and T is the absolute temperature. The concentration profile for electrolyte within the microhole during "open" or "closed" state of the diode is expressed by equation 2.

$$c/c_s = [(c_m/c_s)(1\text{-}e^{-xu/L}) + e^{-xu/L}\text{-}e^{-u}]/(1\text{-}e^{-u}) \quad (2)$$

In this equation the concentration c of electrolyte within the cylindrical region of the microhole (see Figure 15(A)) is given by the limiting concentrations c_m and c_s, the position x, and the length L. Experimental data in Figure 15(C) are presented for three microhole diameters, 5, 10, 20 µm, showing that the match of theory and experiment is good but qualitative. Additional effects are due to external electrolyte gradients, processes within the ionomer and at the ionomer | water interface, chemical reactions that can be driven by the applied potential, non-steady state phenomena, and iR-drop due to the internal cell resistance/ cell geometry [74]. The formation of a pH gradient was demonstrated by monitoring pH in the two compartments close to the graphene oxide ionic diode. At lower electrolyte concentration water heterolysis to protons and hydroxide occurs in competition to the cation transport across the graphene oxide ionomer.

Ionic diode effects have been investigated with novel ion-conducting materials such as polymers of intrinsic microporosity (PIMs [75]). PIM-EA-TB is a polyamine with ethano-anthracene unit (EA) synthesized *via* Tröger base (TB) coupling [76] (see Figure 16). The PIM material is asymmetrically deposited onto a micropore laser-drilled into a PET membrane. The protonation of the PIM-EA-TB backbone occurs at a solution pH < 4 and leads to predominantly anion conduction. Therefore, an anionic diode effect is observed in acidic solution.

Even very thin films of only 300 nm thickness of PIM-EA-TB (on a PET substrate) still resulted in considerable ionic diode effects [77] and a switch from cationic diode for aqueous HCl to anionic diode for aqueous NaOH (Figure 16(D)). Ionic diode current data from PIM-EA-TB diodes clearly show a different type of current-voltage characteristic with a plateau region (see Figure 16(B)). This is believed to be linked to interfacial polarization (at the PIM-EA-TB | aqueous electrolyte interface; see Figure 16(E) and 16(F)), which occurs in addition to the electrolyte accumulation and depletion within the microhole region.

Similar cases of semi-permeable ion conducting materials leading to ionic diode behavior were observed with metal-organic framework (MOF) materials [78], with cellulosic materials [79], with TiO_2 nanosheet films [80], and with biological materials such as M13 bacteriophage aggregate deposits [81]. Figure 17 shows the shape of M13 phage with surface protein defining a positive surface charge when immersed in dilute aqueous acid. When deposited asymmetrically onto a PET support containing a microhole, channels through the deposit are formed from the protein shell of the M13 phage. In acidic

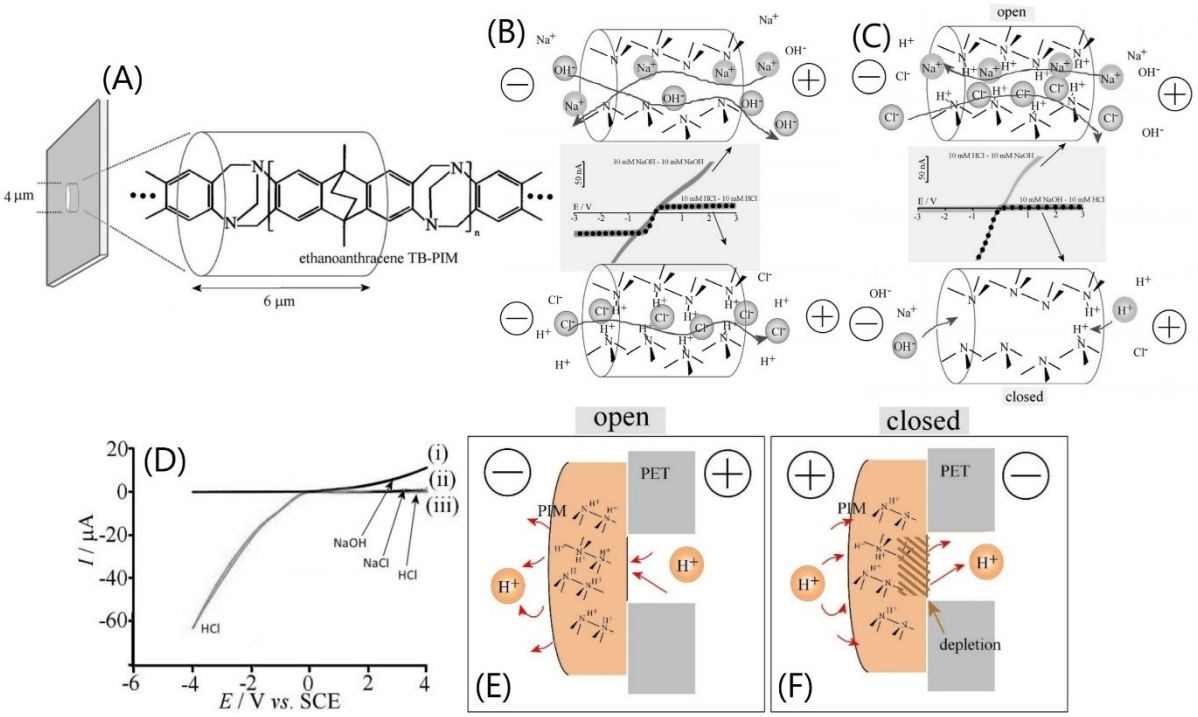

Fig. 16. (A) Molecular structure of PIM-EA-TB. (B) Illustration of ion transport in aqueous NaOH and in aqueous HCl. (C) Illustration of the ionic diode effect when placing aqueous NaOH and HCl on opposite sides of the film. Reprinted with permission from [76]. Copyright (2014) Wiley. (D) Cyclic voltammetry data for scan rate 50 mV s^{-1} and PIM-EA-TB deposited asymmetrically onto a 20 µm diameter microhole in PET immersed in aqueous 10 mM HCl, NaOH, or NaCl. Drawings (E) and (F) show illustrations of the cationic diode effect for PIM-EA-TB in aqueous HCl. Reprinted with permission from [77]. Copyright (2016) Elsevier.

solution, protonation of the protein leads to anionic diode behavior (see Figure 17(E)). Other molecules such as indigo carmine have been proposed to bind into the ion channels. A dip in ionic diode performance was observed for 5 µM indigo carmine and explained with the adsorption of indigo carmine into channels.

Other ionomer materials have been investigated for ionic rectifier effects. Fumasep anion conductor has been shown to give anionic diode phenomena [82] and partially hydrolysed polyacrylonitrile [83] was shown to give a switchable ionic diode with cationic diode behavior in alkaline solution and with anionic ionic diode behavior in acidic solution. Carbon nanofiber based ionic diodes are formed as a result of asymmetric deposition of carbon nanofiber dispersions (in dimethylformamide) to form a nano-mat onto micro-interfaced substrates with varying microhole sizes. Essentially, the nano-mats provide an ion conducting membrane material, while the micro-interface allows ionic current rectification to occur. The carbon nanofiber backbone or pore wall is oxidized to introduce surface charges, which are able to attract or repel mobile ions in solution. Surface oxidised carbon nanofibers allow cationic diode behaviour (see Figure 18 [84]), while amine surface modified carbon nanofibers allow anionic diode behaviour [85]. An interesting case of additional bipolar reactivity is observed particularly for iodide interaction with oxidised carbon nanofibers and localised iodine formation changing the diode behaviour. Diodes made in this way and with additional surface modification are envisaged to be useful in electroanalysis or in ionic diode desalination systems.

5 Potential for Applications of Ionic Rectifiers in Electrochemistry

Electrochemical Desalination. The separation of salt from water poses a technical challenge that requires different types of solutions, depending on the operational scale (plant size scale to supply cities or survival kits for individuals) and depending on the input/output streams and their impact on the environment [86]. Desalination concepts based on ionic rectifiers have been proposed for example using chemically modified nanopore arrays [87]. Ionic diode phenomena could be employed for example for smaller scale water desalination as a means of replacing energy-intensive reverse osmosis [88]. There have been new types of desalination concepts put forward based on new materials such as polymers of intrinsic microporosity (PIM-EA-TB) [89]. When coupling AC driving voltages and a cationic diode and an anionic diode, a two-compartment system would be sufficient (one compartment where the salt concentration decreases and the second compartment where the salt concentration

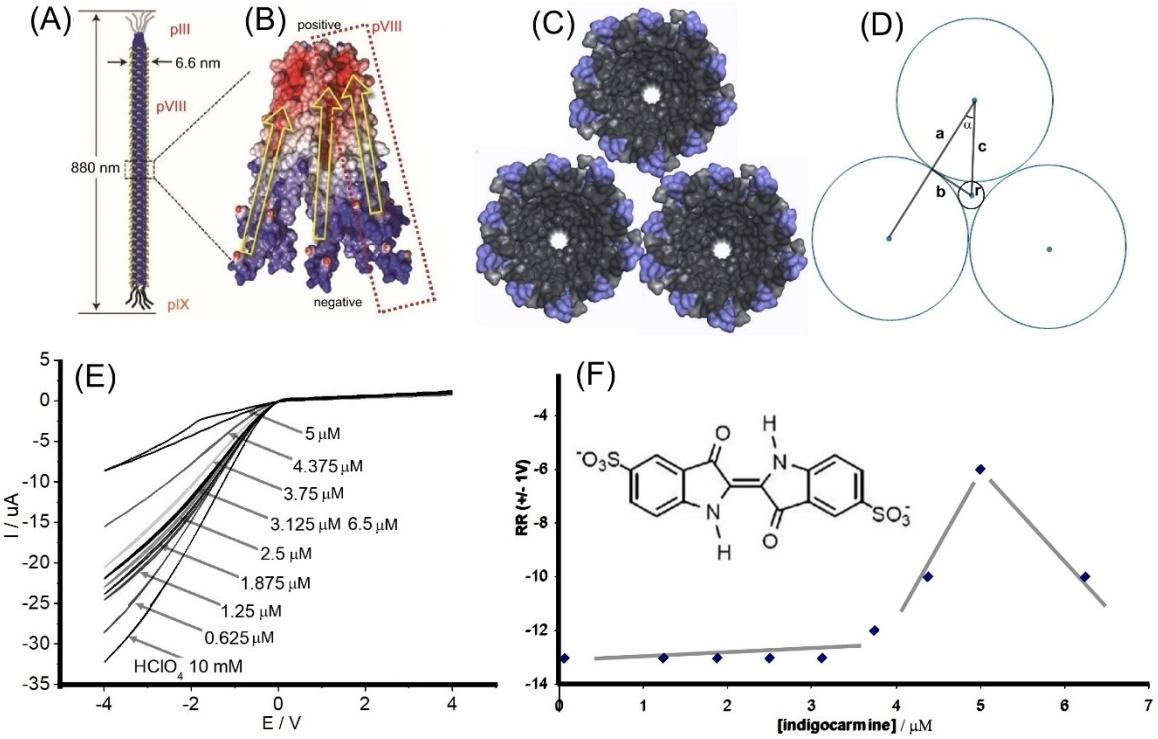

Fig. 17. (A) Drawing of M13 bacteriophage. (B) Illustration of ion channels between bacteriophage. (C, D) Estimation of the ion-channel diameter of approx. $2\,r = 1.0$ nm. (E) Cyclic voltammetry data (scan rate $50\,mV\,s^{-1}$) in aqueous 10 mM $HClO_4$ with small amounts of indigo carmine added. (F) Plot of the rectification ratio at $+/-1$ V as a function of indigo carmine concentration. Reprinted with permission from [81]. Copyright (2020) American Chemical Society.

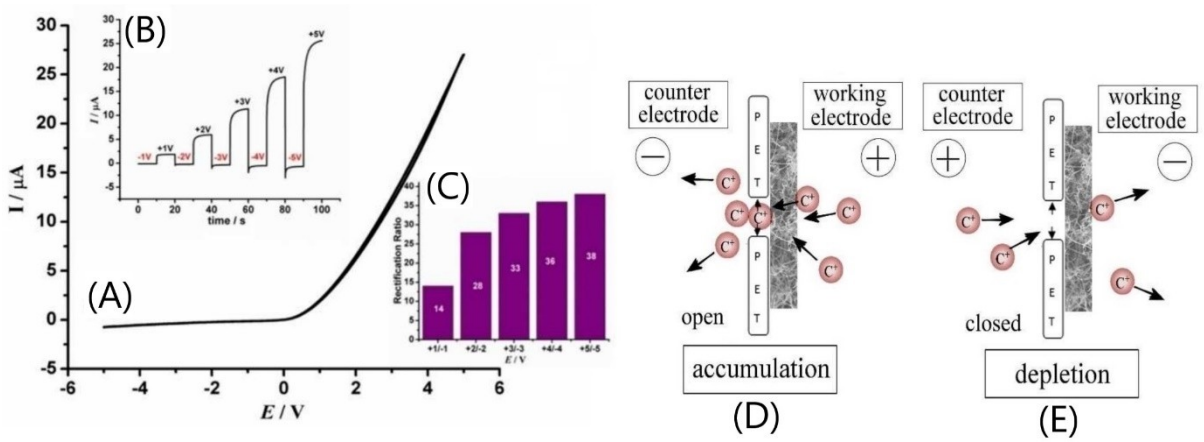

Fig. 18. (A) Cyclic voltammogram for scan rate $50\,mV\,s^{-1}$ and a carbon nano-mat deposited onto a 20 μm diameter microhole in PET. Insets show (B) chronoamperometry transients and (C) a plot of rectification ratio *versus* applied voltage. Drawings in (D) and (E) illustrate the electrolyte accumulation and depletion mechanism. Reprinted with permission from [84]. Copyright (2019) Wiley.

increases). Figure 19 illustrates a possible device based on only one type of rectifier, based on an anionic diode (and cationic resistors, *e.g.* Nafion membranes). In this case a multi-chambered system is required. As drawn, chambers I and VI would retain salt levels and contain the driver electrodes. Chambers II and V will be desalination compartments and chambers III and IV are salination compartments. A similar system based on 4 chambers and based on Nafion cationic diodes has recently been demonstrated [66]. A two-chamber system would be possible when combining a cationic and an anionic diode into a single membrane. Appling AC currents reduces unwanted electrolysis processes (to avoid energy losses) and therefore eliminates problems with hydrogen and chlorine production. This could also offer benefits in areas such as electrodialysis [90], electro-deionisation [91], and

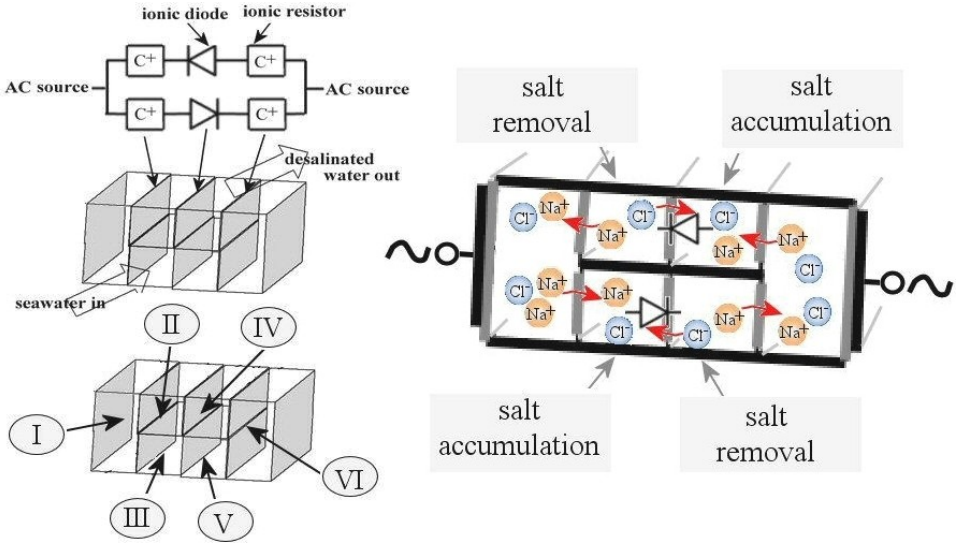

Fig. 19. Schematic drawing of a six-chamber desalination process based on two anionic diodes coupled to four cationic resistors. When AC electricity is applied with external driver electrodes, two chambers undergo desalination whereas two other chambers accumulate salt (reproduced with permission [89]). Reprinted with permission from [89]. Copyright (2015) Royal Society of Chemistry

in capacitive deionization [92]. The challenge of adding ion selectivity into the desalination process will result in future devices that pump specific cations or anions.

Electroanalytical sensors based on ionic diodes. Ionic diodes have much in common with Coulter counters [93,94] and are therefore suitable as amplified ion current detector systems [95]. In particular, nanopore devices are extremely useful as sensors at the single molecule level [96]. A method of DNA base read-out for sequencing DNA could be used as a way of speeding up sequencing, passing aqueous DNA molecules through a nanopore of the same charge has been proven as a quantitative measurement depending on the size and salt concentration of the aqueous solution [97]. A nanopore sequencing technique could also greatly reduce the cost of sequencing [98]. This type of technology is today a commercial reality.

New biosensors made from ionic diode devices [99,100] could simplify the sensor design (avoiding electron transfer; high amplification effect due to ion current sensing; no metal components in the active sensor probe). These new sensors allow individual molecules to pass through a nanoscale pore leading to detectable changes in ionic pore current, based on local changes of the surface charge on walls of single nanopores induced by binding of an analyte. Vlassiouk *et al.* [101] developed a specific biosensing platform based on conical nanofluidic diodes. The tips of the sensors were modified with recognition elements for specific analytes (avidin, streptavidin, and poly γ-D-glutamic acid (γDPGA) from Bacillus anthracis). Binding of the individual analytes changed the surface charge pattern of the system, which was detected as the change in the asymmetric current-voltage curves measured in an aqueous KCl solution. The degree of rectification was used as the detection signal for the presence of an analyte. A proof of concept was provided. To illustrate this concept, Figure 20 depicts the mechanism involved for γDPGA sensing with a nanopore that contained a monoclonal antibody (mAb F26G3) at the tip [101]. The nanopore with mAb F26G3 was incubated with a solution of γDPGA for 3 h, and the current - voltage curves were measured in 10 mM KCl. Depending on the pH of the solution, different surface charge patterns were formed on the pore walls, which led to different *I–V* curves. At pH > 4, γDPGA was negatively charged and thus the current-voltage curves reversed compared to the situation before the γDPGA binding. The system is also shown to provide a new and label-free method for determination of isoelectric points of immobilized proteins. Knowledge of isoelectric points of proteins is very important, as it can improve or impair a biosensing technique.

Ionic diode mechanisms are suitable for sensor development not only in nanopore devices. For example, when forming a "heterojunction" for ionic currents based on two ion conducting polymers, processes at the micro-interface can be analyte concentration sensitive. Putra and co-workers [102] demonstrated an ionic diode device based on a laser-drilled microhole coated with Nafion and with PIM-EA-TB on opposite sides (see Figure 21). Immersed in aqueous salt solutions, this device operated as an ionic diode (dominated by the cationic diode effect from the Nafion). However, when operated in K^+ containing solution with ClO_4^- anions on the opposite side, the increased K^+ concentration at the heterojunction interface caused spontaneous (and reversible) precipitation of $KClO_4$. As a result, a current spike is observed with positive applied potential (the "open" diode state). This current spike was K^+ concentration dependent.

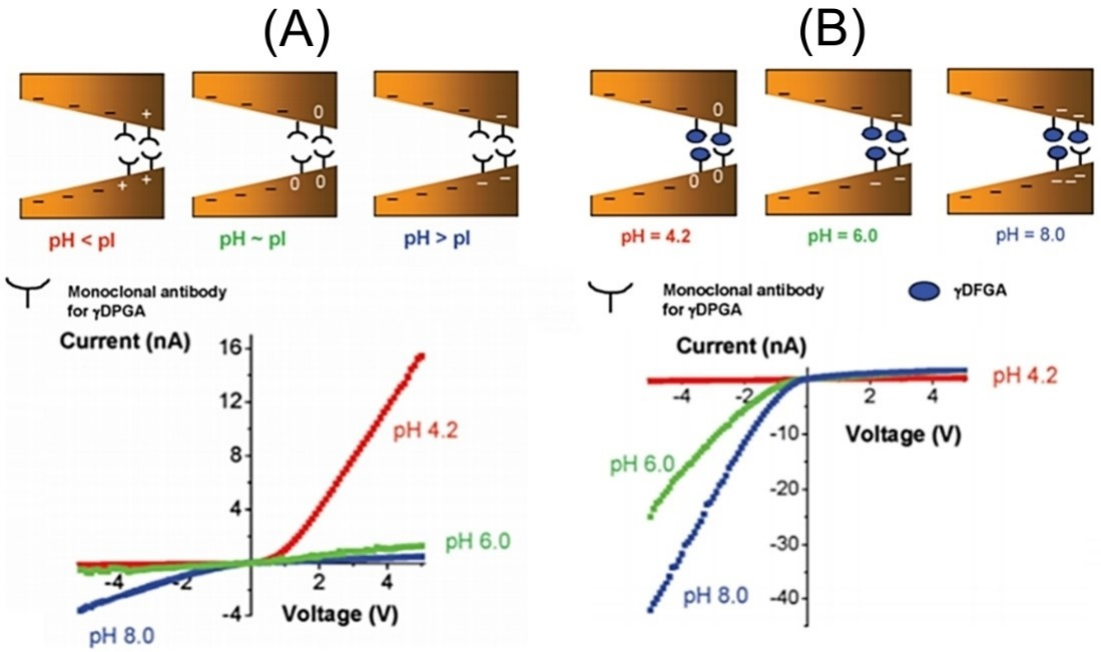

Fig. 20. (A) Effect of electrolyte pH on the monoclonal antibody for detection of the bacterial polyglutamic acid (γDPGA). (B) Sensing γDPGA with a nanopore that contained mAb F26G3 immobilised at the tip. At each pH value distinct ionic diode effects are generated. Reprinted with permission from [101]. Copyright (2009) American Chemical Society.

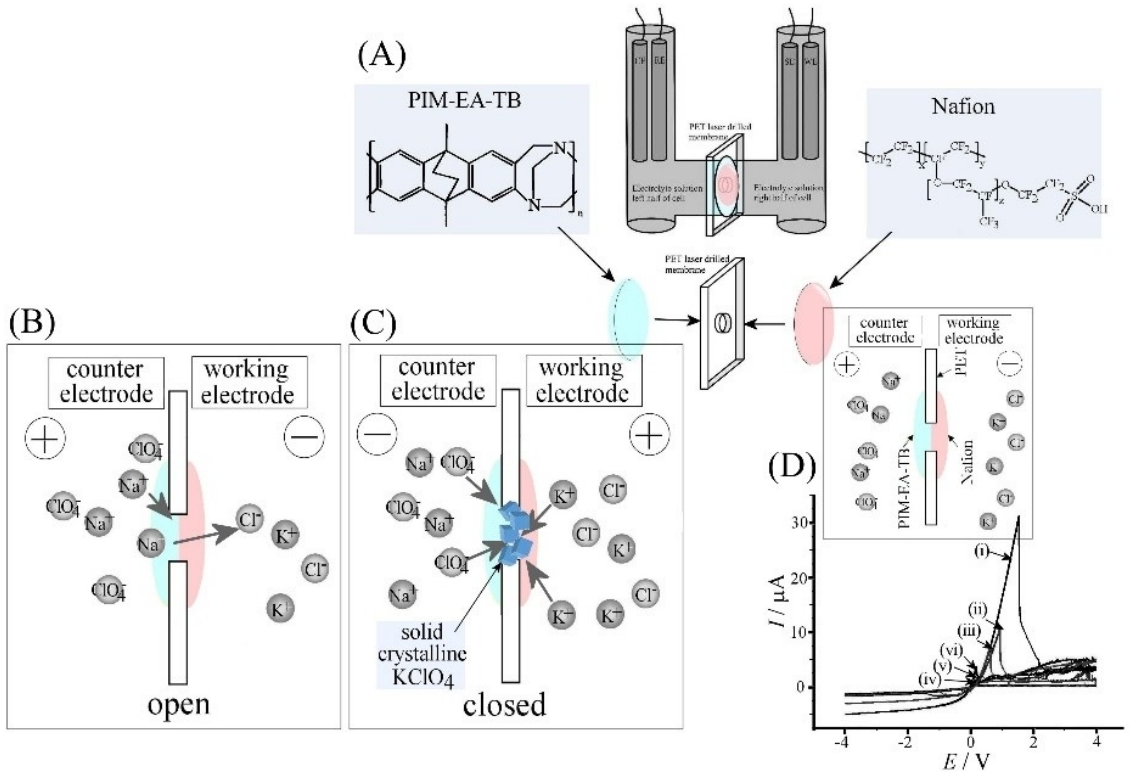

Fig. 21. (A) Schematic of the four-electrode measurement cell with PIM-EA-TB | Nafion heterojunction. (B, C) Schematic drawing of cation and anion transport leading to junction blocking when $KClO_4$ forms. (D) Cyclic voltammetry data (scan rate 25 mV s^{-1}) for the PIM-EA-TB | Nafion heterojunction on a 20 μm diameter microhole in PET immersed in aqueous KCl (with concentration (i) 0.1, (ii) 1.0, (iii) 10, (iv) 100, (v) 500, (vi) 1000 mM in the working electrode compartment) and aqueous $NaClO_4$ (with concentration 0.1 M in the counter electrode compartment). Reprinted with permission from [102]. Copyright (2017) Elsevier.

Photodiodes and energy conversion with ionic diodes. Ionic mechanisms to generate electricity from sunlight have been investigated [103,104], although the photo-excitation in these systems remains fundamentally an electronic (rather than ionic) process. A $Ru(bpy)_3^{2+}$ -based design is illustrated in Figure 22. A sandwich of agarose gels is employed [105]. Illumination with light has been proposed to lead to ion transport and voltage/current output, although efficiencies are low.

The desalination process is endergonic to give pure water and enriched salt water as the two main products. The reversal of this process can be employed for energy production (see "blue energy" from river water and seawater [106]). The appeal for energy production from "hidden solar energy" in river water is considerable [107]. Salinity gradient techniques have been proposed for example based on ionic diodes in heterojunctions of mesoporous carbon (~7 nm, negatively charged) and macro-porous alumina (~80 nm, positively charged). Power output has been predicted but only at an early proof-of-principle level. The ion selectivity of the hetero-junctions is dominated by the mesoporous carbon (see Figure 23). If the salinity gradient is reversed from mesoporous carbon to macro-porous alumina, then the resistance is reduced to 53 %, which supports the idea of the preferential direction for cation transport [108]. Similar to the case of desalination where both DC or AC methods can be developed, for blue energy harvesting AC driven ionic circuits exploiting the rectification effects could be developed to avoid external driver electrode reactions and to make the process continuous.

Another related form of energy conversion could be based on driven chemical processes in which salinity gradients allow production of chemical products (*e.g.* producing hydrogen and oxygen; compare the conversion of ion gradient energy to chemical energy in the ATPase mechanism in nature [109]). Ion transfer at liquid | liquid interfaces has been employed to trigger redox chemical reactions [110], but also bipolar reactions that occur when electrically conducting materials are embedded into the ionic diode will produce chemical products from redox reactions. There are many more opportunities for energy conversion processes in ionic diode and ionic rectifier systems and for applications that mimic natural membrane reactions.

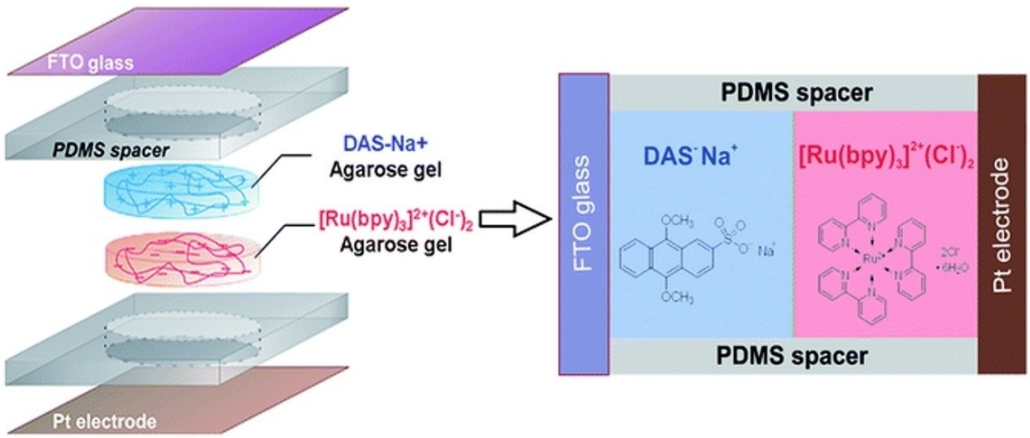

Fig. 22. Schematic of a hydrogel photovoltaic cell using photosensitive dyes to produce the ionic current flow within separate hydrogel layers. Reprinted with permission from [105]. Copyright (2011) Royal Society of Chemistry.

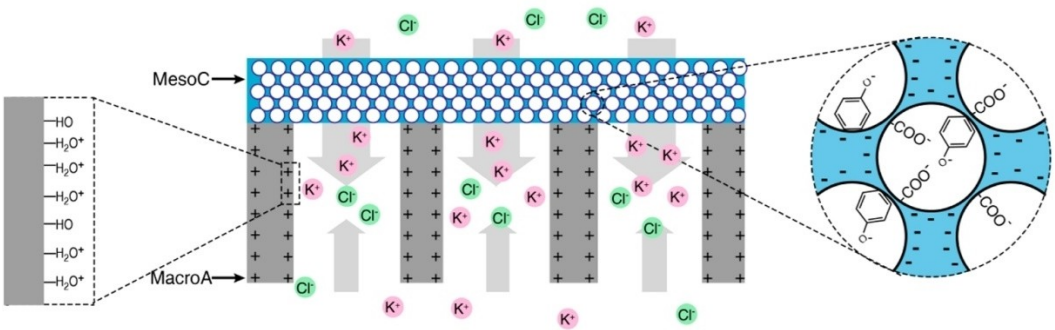

Fig. 23. Schematic representation of how the mesoporous carbon and macroporous alumina selectively allow ion transport to produce the diode effect. Reprinted with permission from [106]. Copyright (2012) American Chemical Society.

6 Conclusions and Outlook

This overview summarises some recent developments based on microscale ionic diodes and it compares various types of ionic diodes, their mechanisms, and possible applications in electrochemical technologies. It has been shown that ionic diode phenomena occur in both nature and in artificial devices. The ion current "rectification effect" can be generated in semipermeable systems based on two prerequisites: (i) asymmetry in the device and (ii) a compositional change linked to the applied external potential.

When using a microhole device, it is possible to employ a "materials approach" to the ionic diode design in which the properties of an ionomer material deposited asymmetrically onto an inert substrate are used to create conditions for high rectification effects. Good ionomer coatings are (i) mechanically robust, (ii) deposited as thin film to give a low ionic resistance, (iii) possess a high charge carrier concentration and mobility, and (iv) do not require extensive and expensive microfabrication compared to solid state single nanopore or track-etched nanopore approaches. In applications based on alternating current (AC) driven processes, the requirement for durability of ionomer materials is high. Fast switching ionic diodes with high rectification ratio will be desirable in order to operate at higher frequencies. Molecular mechanisms for ionic diode switching *e.g.* valve-like processes within nano-channels could be a possible way towards higher frequencies and higher performance. There are many more opportunities for the development of new materials/architectures for ionic diodes to provide fast switching devices with strong rectification effects. This will allow new desalination technology and energy conversion technology to emerge as well as new electroanalytical sensing devices with high amplification effect or chemoreceptive sense/pump systems [95] to be realised.

Acknowledgements

F.M. is grateful for support from the Leverhulme Foundation (RPG-2014-308: "New Materials for Ionic Diodes and Ionic Photodiodes"). A.K.T. thanks the Centre for Sustainable Chemical Technologies (CSCT) and the Engineering and Physical Sciences Research Council (EPSRC) for support. K.M. acknowledges financial support from Provincie Gelderland. M.A.B. acknowledges the EPSRC for funding (Standard Research Studentship, EP/N509498/1). L.T. and O.A.A. acknowledge the financial support of the National Research Foundation, South Africa and the Centre for Nanomaterials Science Research, University of Johannesburg. This work was supported by the Engineering and Physical Sciences Research Council EP/L016354/1.

Data Availability Statement

Data subject to third party restrictions

References

[1] Z. Zhang, X. D. Huang, Y. C. Qian, W. P. Chen, L. P. Wen, L. Jiang, *Adv. Mater.* **2020**, *32*, 1904351.
[2] S. M. Sze, K. K. Ng, *Physics of Semiconductor Devices*, Wiley, New York, **2006**.
[3] R. M. Metzger, D. L. Mattern, *Unimolecular and Supramolecular Electronics II. Topics in Current Chemistry*, vol 313. Springer, **2011**, Berlin.
[4] Z. Zhang, L. P. Wen, L. Jiang, *Chem. Soc. Rev.* **2018**, *47*, 322.
[5] Z. Y. Meng, J. Zhai, *Curr. Org. Chem.* **2018**, *22*, 737.
[6] B. D. B. Aaronson, D. P. He, E. Madrid, M. A. Johns, J. L. Scott, L. Fan, J. Doughty, M. A. S. Kadowaki, I. Polikarpov, N. B. McKeown, F. Marken, *ChemistrySelect* **2017**, *2*, 871.
[7] W. H. Guan, S. X. Li, M. A. Reed, *Nanotechnology* **2014**, *25*, 122001.
[8] L. J. Cheng, L. J. Guo, *Chem. Soc. Rev.* **2010**, *39*, 923.
[9] X. D. Huang, X. Y. Kong, L. P. Wen, L. Jiang, *Adv. Funct. Mater.* **2018**, *28*, 1801079.
[10] W. J. Lan, M. A. Edwards, L. Luo, R. T. Perera, X. J. Wu, C. R. Martin, H. S. White, *Acc. Chem. Res.* **2016**, *49*, 2605.
[11] J. Experton, X. J. Wu, C. R. Martin, *Nanomaterials* **2017**, *7*, 445.
[12] J. A. Cooper, S. Borsley, P. J. Lusby, S. L. Cockroft, *Chem. Sci.* **2017**, *8*, 5005.
[13] B. Doherty, *MicroNotes*: PIN Diode Fundamentals, Watertown, MA: Microsemi Corp. MicroNote Series 701.
[14] K. M. Gupta, N. Gupta, *Advanced Semiconducting Materials and Devices*, Book Series: Engineering Materials, **2016**, 235–259.
[15] H. P. Agarwal, J. O'M. Bockris, R. E. White, B. E. Conway, *Modern Aspects of Electrochemistry*, eds. No. 20 pp 177–263, **1989**.
[16] R. P. Buck, N. A. Surridge, R. W. Murray, *J. Electrochem. Soc.* **1992**, *139*, 136.
[17] B. Katz, *J. Physiol.*, **1942**, *100*, 369.
[18] R. Guttman, *J. Gen. Physiol.*, **1944**, *28*, 43.
[19] K. Cooper, E. Jakobsson, P. Wolynes, *Prog. Biophys. Mol. Biol.* **1985**, *46*, 51.
[20] A. L. Hodgkin, A. F. Huxley, *J. Physiol.* **1952**, *117*, 500.
[21] A. L. Hodgkin, R. D. Keynes, *J. Physiol.* **1955**, *128*, 28.
[22] A. L. Hodgkin, R. D. Keynes, *J. Physiol.* **1955**, *128*, 61.
[23] O. Sten-Knudsen, *Biological Membranes*, Cambridge University Press, **2002**.
[24] D. Oliver, T. Baukrowitz, B. Fakler, *Eur. J. Biochem.* **2000**, *267*, 5824.
[25] A. Alcaraz, P. Ramirez, E. Garcia-Gimenez, M. L. Lopez, A. Andrio, V. M. Aguilella, *J. Phys. Chem. B* **2006**, *110*, 21205.
[26] C. S. Fuller, *Recent Chemical Progress*, **1956**, *17*, 75.
[27] B. Lovrecek, A. Despic, J. Bockris, *J. Phys. Chem.* **1959**, *63*, 750.
[28] H. Chun, T. D. Chung, *Ann. Rev. Anal. Chem.* **2015**, *8*, 441.
[29] H. J. Koo, O. D. Velev, *Biomicrofluidics* **2013**, *7*, 031501.
[30] M. Ali, P. Ramirez, S. Nasir, J. Cervera, S. Mafe, W. Ensinger, *Soft Matter* **2019**, *15*, 9682.
[31] L. Hegedus, N. Kirschner, M. Wittmann, Z. Noszticzius, *J. Phys. Chem. A* **1998**, *102*, 6491.
[32] S. K. Jana, S. Banerjee, S. Bayan, H. R. Inta, V. Mahalingam, *J. Phys. Chem. C* **2018**, *122*, 11378.
[33] M. Lepoitevin, T. J. Ma, M. Bechelany, J. M. Janot, S. Balme, *Adv. Colloid Interface Sci.* **2017**, *250*, 195.
[34] J. W. Bai, D. Q. Wang, S. W. Nam, H. B. Peng, R. Bruce, L. Gignac, M. Brink, E. Kratschmer, S. Rossnagel, P.

Waggonerl, K. Reuter, C. Wang, Y. Astier, V. Balagurusamy, B. Q. Luan, Y. Kwark, E. Joseph, M. Guillorn, S. Polonsky, A. Royyuru, S. P. Rao, G. Stolovitzky, *Nanoscale*, **2014**, *6*, 8900.
[35] T. Ma, J. M. Janot, S. Balme, *Small Methods* **2020**, *4*, 2000366.
[36] Y. Choi, L. A. Baker, H. Hillebrenner, C. R. Martin, *Phys. Chem. Chem. Phys.* **2006**, *8*, 4976.
[37] Z. Siwy, Y. Gu, H. A. Spohr, D. Baur, A. Wolf-Reber, R. Spohr, Y. E. Korchev, *EPL* **2002**, *60*, 349.
[38] C. C. Harrell, Z. Siwy, C. R. Martin, *Small* **2006**, *2*, 194.
[39] H. S. White, A. Bund, *Langmuir* **2008**, *24*, 2212.
[40] M. Ali, P. Ramirez, H. Q. Nguyen, S. Nasir, J. Cervera, S. Mafe, W. Ensinger, *ACS Nano* **2012**, *6*, 3631.
[41] Z. Siwy, E. Heins, C. C. Harrell, P. Kohli, C. R. Martin, *J. Am. Chem. Soc.* **2004**, *126*, 10850.
[42] I. Vlassiouk, S. Smirnov, Z. Siwy, *ACS Nano* **2008**, *2*, 1589.
[43] R. Karnik, C. Duan, K. Castelino, H. Daiguji, A. Majumdar, *Nano Lett.* **2007**, *7*, 547.
[44] Y. L. Xu, X. Sui, S. Guan, J. Zhai, L. C. Gao, *Adv. Mater.* **2015**, *27*, 1851.
[45] G. S. B. Suh, A. M. Wong, A. C. Hergarden, *Nature* **2004**, *431*, 854.
[46] E. A. Hallem, P. W. Stemberg, *PNAS* **2008**, *105*, 8038.
[47] E. C. Yusko, R. An, M. Mayer, *ACS Nano* **2010**, *4*, 477.
[48] X. He, K. Zhang, T. Li, Y. Jiang, P. Yu, L. Mao, *J. Am. Chem. Soc.* **2017**, *139*, 1396.
[49] W. Ouyang, J. Han, W. Wang, *Lab Chip* **2017**, *17*, 3006.
[50] F. F. Liu, X. P. Zhao, B. Kang, X. H. Xia, C. Wang, *TRAC* **2020**, *123*, 115760.
[51] R. A. Lucas, C.-Y. Lin, Z. S. Siwy, *J. Phys. Chem. B* **2019**, *123*, 6123.
[52] Y. F. Liu, L. Yobas, *Biosens. Bioelectron.* **2013**, *50*, 78.
[53] K. Sint, B. Wang, P. Kral, *J. Am. Chem. Soc.* **2008**, *130*, 16448.
[54] Z. J. He, J. Zhou, X. H. Lu, B. Corry, *ACS Nano* **2013**, *7*, 10148.
[55] M. Tagliazucchi, I. Szleifer, *Mater. Today* **2015**, *18*, 131.
[56] Y. A. P. Sirkin, M. Tagliazucchi, I. Szleifer, *Mater. Today* **2020**, *5*, 100047.
[57] O. J. Cayre, S. T. Chang, O. D. Velev, *J. Am. Chem. Soc.* **2007**, *129*, 10801.
[58] L. L. Wang, H. C. Zhang, Z. Yang, J. J. Zhou, L. P. Wen, L. Li, L. Jiang, *Phys. Chem. Chem. Phys.* **2015**, *17*, 6367.
[59] R. Zhao, G. H. He, Y. L. Deng, *Electrochem. Commun.* **2012**, *23*, 106.
[60] E. C. Yusko, R. An, M. Mayer, *ACS Nano* **2010**, *4*, 477.
[61] G. Yossifon, P. Mushenheim, Y. C. Chang, H. C. Chang, *Phys. Rev. E* **2009**, *79*, 046305.
[62] G. Yossifon, Y.-C. Chang, *Phys. Rev. Lett.* **2009**, *103*, 154502.
[63] I. W. Leong, M. Tsutsui, S. Murayama, Y. H. He, M. Taniguchi, *J. Phys. Chem. B* **2020**, *124*, 7086.
[64] J. Experton, X. J. Wu, C. R. Martin, *Nanomaterials* **2017**, *7*, 445.
[65] H. C. Feng, H. L. Chang, X. Zhong, T. N. Wong, *Adv. Colloid Interface Sci.* **2020**, *280*, 102159.
[66] B. R. Putra, E. Madrid, L. Tshwenya, O. A. Arotiba, F. Marken, *Desalination* **2020**, *480*, 114351.
[67] H. J. Lee, P. D. Beattie, B. J. Seddon, M. D. Osborne, H. H. Girault, *J. Electroanal. Chem.* **1997**, *440*, 73.
[68] A. M. Bond, *Analyst* **1994**, *119*, R1.
[69] F. Reymond, D. Fermin, H. J. Lee, H. H. Girault, *Electrochim. Acta* **2000**, *45*, 15.
[70] R. Brown, E. Madrid, R. Castaing, J. M. Stone, A. M. Squires, K. J. Edler, K. Takashina, F. Marken, *ChemElectroChem* **2017**, *4*, 1172.
[71] D. P. He, E. Madrid, B. D. B. Aaronson, L. Fan, J. Doughty, K. Mathwig, A. M. Bond, N. B. McKeown, F. Marken, *ACS Appl. Mater. Interfaces* **2017**, *9*, 11272.
[72] K. Mathwig, B. D. B. Aaronson, F. Marken, *ChemElectroChem* **2018**, *5*, 897.
[73] B. R. Putra, K. J. Aoki, J. Y. Chen, F. Marken, *Langmuir* **2019**, *35*, 2055.
[74] K. J. Aoki, L. Liu, F. Marken, J. Y. Chen, *Electrochim. Acta* **2020**, *358*, 136839.
[75] L. N. Wang, Y. Z. Zhao, B. B. Fan, M. Carta, R. Malpass-Evans, N. B. McKeown, F. Marken, *Electrochem. Commun.* **2020**, *118*, 106798.
[76] E. Madrid, Y. Y. Rong, M. Carta, N. B. McKeown, R. Malpass-Evans, G. A. Attard, T. J. Clarke, S. H. Taylor, Y. T. Long, F. Marken, *Angew. Chem. Int. Ed.* **2014**, *53*, 10751.
[77] Y. Y. Rong, Q. L. Song, K. Mathwig, E. Madrid, D. P. He, R. G. Niemann, P. J. Cameron, S. E. C. Dale, S. Bending, M. Carta, R. Malpass-Evans, N. B. McKeown, F. Marken, *Electrochem. Commun.* **2016**, *69*, 41.
[78] E. Madrid, M. A. Buckingham, J. M. Stone, A. T. Rogers, W. J. Gee, A. D. Burrows, P. R. Raithby, V. Celorrio, D. J. Fermin, F. Marken, *Chem. Commun.* **2016**, *52*, 2792.
[79] B. D. B. Aaronson, D. Wigmore, M. A. Johns, J. L. Scott, I. Polikarpov, F. Marken, *Analyst* **2017**, *142*, 3707.
[80] B. R. Putra, C. Harito, D. V. Bavykin, F. C. Walsh, W. T. Wahyuni, J. A. Boswell, A. M. Squires, J. M. F. Schmitt, M. A. Da Silva, K. J. Edler, P. J. Fletcher, A. E. Gesell, F. Marken, *J. Solid State Electrochem.* **2019**, *23*, 1237.
[81] B. R. Putra, K. Szot-Karpińska, P. Kudła, H. Yin, J. A. Boswell, A. M. Squires, M. A. Da Silva, K. J. Edler, P. J. Fletcher, S. C. Parker, F. Marken, *ACS Appl. Bio Mater.* **2020**, *3*, 512.
[82] L. Tshwenya, O. Arotiba, B. R. Putra, E. Madrid, K. Mathwig, F. Marken, *J. Electroanal. Chem.* **2018**, *815*, 114.
[83] L. Tshwenya, F. Marken, K. Mathwig, O. A. Arotiba, *ACS Appl. Mater. Interfaces* **2020**, *12*, 3214.
[84] L. Tshwenya, K. Marken, O. A. Arotiba, *ChemElectroChem* **2019**, *6*, 3145.
[85] L. Tshwenya, B. R. Putra, B. O. Orimolade, F. Marken, O. A. Arotiba, *Electrochim. Acta* **2020**, *354*, 136750.
[86] K. Elsaid, M. Kamil, E. T. Sayed, M. A. Abdelkareem, T. Wilberforce, A. Olabi, *Sci. Total Environ.* **2020**, *748*, 141528.
[87] K. Xiao, L. Chen, Z. Zhang, G. H. Xie, P. Li, X. Y. Kong, L. P. Wen, L. Jiang, *Angew. Chem. Int. Ed.* **2017**, *56*, 8168.
[88] J. Zhou, V. W. Chang, A. G. Fane, *Water Res.* **2014**, *61*, 210.
[89] E. Madrid, P. Cottis, Y. Y. Rong, A. T. Rogers, J. M. Stone, R. Malpass-Evans, M. Carta, N. B. McKeown, F. Marken, *J. Mater. Chem. A* **2015**, *3*, 15849.
[90] H. Strathmann, *Desalination*, **2010**, *264*, 268.
[91] L. Alvarado, A. Chen, *Electrochim. Acta* **2014**, *132*, 583.
[92] S. Porada, R. Zhao, A. van der Wal, V. Presserd, P. M. Biesheuvel, *Prog. Mater. Sci.* **2013**, *58*, 1388.
[93] R. R. Henriquez, T. Ito, L. Sun, R. M. Crooks, *Analyst* **2004**, *129*, 478.
[94] J. J. Kasianowicz, J. W. F. Robertson, E. R. Chan, J. E. Reiner, V. M. Stanford, *Ann. Rev. Anal. Chem.* **2008**, *1*, 737.
[95] S. N. Bush, T. Volta, C. R. Martin, *Nanomaterials* **2020**, *10*, 571.
[96] S. Howorka, Z. Siwy, *Chem. Soc. Rev.* **2009**, *38*, 2360.

[97] Y. H. He, M. Tsutsui, C. Fan, M. Taniguchi, T. Kawai, *ACS Nano* **2011**, *5*, 5509.
[98] D. Branton, D.W Deamer, A. Marziali, H. Bayley, S. A. Benner, T. Butler, M. Di Ventra, S. Garaj, A. Hibbs, X. H. Huang, S. B. Jovanovich, P. S. Krstic, S. Lindsay, X. S. S. Ling, C. H. Mastrangelo, A. Meller, J. S. Oliver, Y. V. Pershin, J. M. Ramsey, R. Riehm, G. V. Soni, V. Tabard-Cossa, M. Wanunu, M. Wiggin, J. A. Schloss, *Nature Biotechnol.* **2008**, *26*, 1146.
[99] Z. Y. Meng, J. Zhai, *Curr. Org. Chem.* **2018**, *22*, 737.
[100] O. M. Eggenberger, C. F. Ying, M. Mayer, *Nanoscale* **2019**, *11*, 19636.
[101] I. Vlassiouk, T. R. Kozel, Z. S. Siwy, *J. Am. Chem. Soc.* **2009**, *131*, 8211.
[102] B. R. Putra, M. Carta, R. Malpass-Evans, N. B. McKeown, F. Marken, *Electrochim. Acta* **2017**, *258*, 807.
[103] X. D. Huang, X. Y. Kong, L. P. Wen, L. Jiang, *Adv. Funct. Mater.* **2018**, *28*, 1801079.
[104] W. White, C. D. Sanborn, D. M. Fabian, S. Ardo, *Joule*, **2018**, *2*, 94.
[105] H. J. Koo, S. T. Chang, J. M. Slocik, R. R. Naik, O. D. Velev, *J. Mater. Chem.* **2011**, *21*, 72.
[106] J. Gao, W. Guo, D. Feng, H. T. Wang, D. Y. Zhao, L. Jiang, *J. Am. Chem. Soc.* **2014**, *136*, 12265.
[107] T. J. Ma, E. Balanzat, J. M. Janot, S. Balme, *ACS Appl. Mater. Interfaces* **2019**, *11*, 12578.
[108] L. X. Cao, W. Guo, Y. G. Wang, L Jiang, *Langmuir* **2012**, *28*, 2194.
[109] P. D. Vogel, *Eur. J. Pharm. Biopharm.* **2005**, *60*, 267.
[110] A. N. J. Rodgers, S. G. Booth, R. A. W. Dryfe, *Electrochem. Commun.* **2014**, *47*, 17.
[111] H. Chun, T. D. Chung, *Ann. Rev. Anal. Chem.* **2015**, *8*, 441.

Received: January 27, 2021
Accepted: February 21, 2021
Published online on ■■, ■■

REVIEW

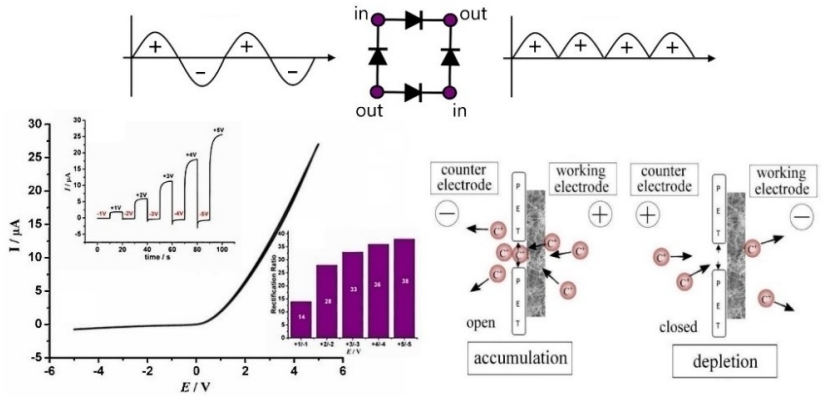

*B. Riza Putra, L. Tshwenya, M. A. Buckingham, J. Chen, K. Jeremiah Aoki, K. Mathwig, O. A. Arotiba, A. K. Thompson, Z. Li, F. Marken**